Entergy

Entergy Operations, Inc.
1340 Echelon Parkway
Jackson, Mississippi 39213-8298
Tel 601-368-5758

F. G. Burford
Acting Director
Nuclear Safety & Licensing

CNRO-2006-00039

August 31, 2006

U. S. Nuclear Regulatory Commission
Attn.: Document Control Desk
Washington, DC 20555-0001

SUBJECT: Results of the Waterford 3 Pressurizer Flaw Evaluation

Waterford Steam Electric Station, Unit 3
Docket No. 50-382
License No. NPF-38

REFERENCES:

1. Entergy Operations, Inc. letter CNRO-2006-00037 to the NRC dated July 31, 2006
2. Entergy Operations, Inc. letter W3F1-2006-0043 to the NRC dated August 29, 2006

Dear Sir or Madam:

In Reference 1, Entergy Operations, Inc. (Entergy) committed to provide to the NRC staff the results of the flaw evaluation performed on the pressurizer at Waterford Steam Electric Station, Unit 3 (Waterford 3). The purpose of this evaluation was to qualify the Waterford 3 pressurizer with respect to recently-identified insurge/outsurge transient loading conditions. Entergy has completed this evaluation and, as committed, is providing it to the staff via the enclosure to this letter. This evaluation is being provided for information only.

Regarding the Waterford 3 pressurizer, Entergy transmitted to the NRC a summary of the small-bore nozzle repairs via Reference 2.

Should you have any questions regarding this letter, please contact Guy Davant at (601) 368-5756.

This letter contains no commitments.

Very truly yours,

FGB/GHD/ghd
Enclosure: Fracture Mechanics Evaluation of Potential Remnant Crack in Waterford 3 Pressurizer Small Bore Nozzles

A047

cc: Mr. W. A. Eaton (ECH) (w/o enclosure)
Mr. J. E. Venable (W3) (w/o enclosure)

Dr. Bruce. S. Mallett
Regional Administrator, Region IV
U. S. Nuclear Regulatory Commission
611 Ryan Plaza Drive, Suite 400
Arlington, TX 76011-8064

NRC Senior Resident Inspector (w/o enclosure)
Waterford Steam Electric Station, Unit 3
P. O. Box 822
Killona, LA 70066

U. S. Nuclear Regulatory Commission
Attn: Mr. M. B. Fields
MS O-7 D1
Washington, DC 20555-0001

ENCLOSURE

CNRO-2006-00039

Fracture Mechanics Evaluation of Potential Remnant Crack in Waterford 3 Pressurizer Small Bore Nozzles

Report No.: SIR-06-302
Revision No.: 1
Project No.: WSES-16Q
File No.: WSES-16Q-401
August 2006

Fracture Mechanics Evaluation of Potential Remnant Crack in Waterford-3 Pressurizer Small Bore Nozzles

Prepared for:

Entergy Operations, Inc.

Contract No. 10118033

Prepared by:

Structural Integrity Associates, Inc.
San Jose, California

Prepared by: G. Angah Miessi — Date: 8/24/06

Reviewed by: Charles J. Fourcade — Date: 8/24/06

Approved by: Richard A. Mattson, P.E. — Date: 8/24/06

REVISION CONTROL SHEET

Document Number: SIR-06-302

Title: Fracture Mechanics Evaluation of Potential Remnant Crack in Waterford-3 Pressurizer Small Bore Nozzles

Client: Entergy Operations, Inc.

SI Project Number: WSES-16Q

Section	Pages	Revision	Date	Comments
1.0 2.0 3.0 4.0 5.0 6.0 7.0	1-1 2-1 – 2-5 3-1 – 3-10 4-1 – 4-15 5-1 – 5-11 6-1 7-1 – 7-2	0	7/18/06	Initial Issue
2.0 3.0 7.0	2-2 – 2-6 3-3 7-2	1	8/24/06	Added Cooldown Transient Description for Top Head Instrument Nozzle

Table of Contents

Section		Page
1.0	Introduction	1-1
2.0	Finite Element Analyses	2-1
2.1	Finite Element Models	2-1
2.2	Stress Analyses	2-1
3.0	linear elastic fracture mechanics	3-1
3.1	Stress Intensity Factors	3-1
3.2	Allowable Stress Intensity Factors	3-2
3.3	Stress Intensity Factors Comparison	3-3
4.0	Elastic-Plastic Fracture Mechanics	4-1
4.1	Material J-Resistance Curve	4-2
4.2	Calculation of Applied J-T	4-4
4.3	Results of EPFM Analysis	4-5
5.0	Fatigue Crack Growth Analysis	5-1
5.1	Fatigue Cycle Definition	5-1
5.2	Postulated Flaws	5-1
5.3	Stress Intensity Factor Distribution	5-2
5.4	Fatigue Crack Growth Law	5-2
5.5	Results of Fatigue Crack Growth Analysis	5-3
6.0	Conclusion	6-1
7.0	References	7-1

List of Tables

Table | Page

Table 3-1 LEFM Results – Bottom Head Heater Sleeve Nozzle 3-4

Table 3-2 LEFM Results – Top Head Instrument Nozzle 3-5

Table 3-3 LEFM Results Summary – Side Shell Temperature Instrument Nozzle 3-6

Table 3-4 LEFM Results Summary – Top Head Instrument Nozzle 3-6

Table 4-1 J-T Instability Computations – Heater Sleeve Nozzle 4-7

Table 4-2 J-T Instability Computations – Top Head Instrument Nozzle 4-8

Table 5-1 Plant Design Transients for Pressurizer Bottom Head Nozzles 5-4

Table 5-2 Plant Design Transients for Pressurizer Side Shell Nozzles 5-5

Table 5-3 Plant Design Transients for Pressurizer Top Head Instrument Nozzle 5-5

Table 5-4 Fatigue Crack Growth Results – Bottom Head Heater Sleeve Nozzle 5-6

Table 5-5 Fatigue Crack Growth Results – Bottom Head Instrument Nozzle 5-7

Table 5-6 Fatigue Crack Growth Results – Side Shell Temperature Instrument Nozzle 5-8

Table 5-7 Fatigue Crack Growth Results – Top Head Instrument Nozzle 5-8

List of Figures

Figure | Page

Figure 2-1. Pressurizer Bottom Head Finite Element Model 2-4
Figure 2-2. Pressurizer Side Shell Temperature Nozzle Finite Element Model 2-5
Figure 2-3. Pressurizer Top Head Instrument Nozzle Finite Element Model 2-6
Figure 3-1. Pressurizer Heater Sleeve Nozzle Postulated Flaw Dimensions (Flawed Portion shown in Magenta) (Flaw 1) 3-7
Figure 3-2. Pressurizer Bottom Head Instrument Nozzle Postulated Flaw Dimensions (Flawed Portion shown in Magenta) 3-8
Figure 3-3. Pressurizer Side Shell Temperature Nozzle Flaw Dimensions 3-9
Figure 3-4. Pressurizer Top Head Instrument Nozzle Initial Flaw 3-10
Figure 4-1. Schematic of EPFM Stability Analysis from ASME Code, Section XI, Appendix K 4-9
Figure 4-2. J-T Diagram for Several Reactor Vessel Steels and Welds Showing Rough Correlation with Charpy V-notch Upper Shelf Energy 4-9
Figure 4-3. Correlation of Coefficient C of Power Law J-R Curve Representation with Charpy V-notch Upper Shelf Energy 4-10
Figure 4-4. Correlation of Exponent m of Power Law J-R Curve Representation with Coefficient C and Flow Stress σ_0 4-10
Figure 4-5. Fitted Charpy V-notch Data for Waterford-3 Vessel Surveillance Plate and Pressurizer Bottom Head Plate Showing 95% Prediction Limits 4-11
Figure 4-6. J-T Diagram for EPFM Stability Analysis – Heater Sleeve Nozzle Penetration at Uphill Location, Largest Modeled Flaw 4-12
Figure 4-7. J-T Diagram for EPFM Stability Analysis – Heater Sleeve Nozzle Penetration at Downhill Location, Largest Modeled Flaw 4-12
Figure 4-8. J-T Diagram for EPFM Stability Analysis – Bottom Head Instrument Nozzle at Uphill Location, Largest Modeled Flaw 4-13
Figure 4-9. J-T Diagram for EPFM Stability Analysis – Bottom Head Instrument Nozzle at Downhill Location, Largest Modeled Flaw 4-13
Figure 4-10. J-T Diagram for EPFM Stability Analysis – Heater Sleeve Nozzle Penetration at Downhill Location, End of Evaluation Period Flaw 4-14
Figure 4-11. J-T Diagram for EPFM Stability Analysis – Bottom Head Instrument Nozzle at Uphill Location, End of Evaluation Period Flaw 4-14
Figure 4-12. J-T Diagram for EPFM Stability Analysis – Bottom Head Instrument Nozzle at Downhill Location, End of Evaluation Period Flaw 4-15
Figure 5-1. Fatigue Crack Growth Results, Bottom Head Heater Sleeve Nozzle Uphill and Downhill Locations 5-9
Figure 5-2. Fatigue Crack Growth Results, Bottom Head Instrument Nozzle Uphill and Downhill Locations 5-10
Figure 5-3. Fatigue Crack Growth Results, Side Shell Temperature Nozzle 5-11
Figure 5-4. Fatigue Crack Growth Results, Top Head Instrument Nozzle 5-11

1.0 INTRODUCTION

Small bore nozzles in the Waterford-3 pressurizer that are fabricated from Alloy 600 material and attached to the pressurizer shell with Alloy 182 J-groove welds are susceptible to primary water stress corrosion cracking (PWSCC). In particular, the following small bore nozzles of the Waterford-3 pressurizer are considered in this report:

- Bottom Head Heater Sleeve Nozzle
- Bottom Head Instrument Nozzle
- Side Shell Temperature Nozzle
- Top Head Instrument Nozzle

Two types of repair designs can be used for such nozzles to prevent leakage in the event of nozzle attachment weld degradation due to PWSCC. The first repair design is an OD repair pad which consists of welding a new, PWSCC resistant, Alloy 690 nozzle to a weld build-up pad on the outside diameter of the pressurizer. The second repair design is the mid-wall repair whereby a new, PWSCC resistant, Alloy 690 nozzle is welded to the low alloy steel pressurizer shell within the bore hole. Since in both repair designs, a portion of the old nozzle is left in place and the J-grove weld is not repaired, there is the potential that a remnant flaw in the J-groove weld could propagate through the pressurizer vessel wall. Therefore, a fracture mechanics analysis is performed to ensure that this remnant flaw would remain stable.

The fracture mechanics evaluation of the potential remnant crack in the Waterford-3 pressurizer small bore nozzles is summarized in this report. For the bottom head heater sleeve nozzle, the fracture mechanics analyses have been performed on the outermost nozzle, which is the controlling nozzle for all other heater sleeves. Since postulated cracking on the inside surface is being evaluated, results documented herein are pertinent to both of the repair techniques described above even though the analyses for a particular nozzle may have been done with only one of the repair designs.

2.0 FINITE ELEMENT ANALYSES

Finite element stress analyses were performed to support the repair designs for the pressurizer small bore nozzles. The finite element stress analyses performed for each of the small bore nozzles included in this evaluation are documented in detail in calculation packages [1-4 and 23-25]. All pertinent loading conditions, including applicable thermal transients, were analyzed. The stress information resulting from these finite element analyses was incorporated into the fracture mechanics analyses of the pressurizer nozzles.

2.1 Finite Element Models

A three-dimensional finite element model was built for each of the four pressurizer small bore nozzles being evaluated. In the cases of the bottom head nozzles, the model included the lower hemispherical head of the pressurizer, the surge nozzle and its thermal sleeve, the support skirt, the interior surface cladding on both the vessel and surge nozzle, all the heater sleeve and instrumentation penetrations and the associated J-groove weld attachments. The finite element model is shown in Figure 2-1. As illustrated in Figures 2-2 and 2-3, in the cases of the side shell and top head nozzles, the finite element models included portions of the pressurizer vessel, the interior surface cladding, the temperature or instrument nozzle and the attachment J-groove weld.

2.2 Stress Analyses

Finite element stress analyses were performed to determine the stress distributions in each of the pressurizer nozzles under consideration. Internal pressure and applicable thermal transient loads were applied to the finite element models described above. Residual stresses due to the application of the cladding in the pressurizer vessel, the subsequent post-weld heat treatment, the J-groove weld and the hydrostatic pressure testing were also computed. A number of different transient conditions were evaluated. These are summarized as follows:

- Heatup Thermal Transient

  The heatup thermal transient was based on the most conservative combination of insurge/outsurge events as described in Table 4 and Figure 4 of Reference 5.

- Cooldown Thermal Transient

  The cooldown thermal transient was based on the most conservative combination of insurge/outsurge events as described in Table 3 and Figure 2 of Reference 5. For the final entry, instead of holding at 445°F as indicated in Reference 5, the transient ends with a 200°F/hr cooldown to a final temperature of 70°F.

  For the top head instrument nozzle, the cooldown transient is based on Reference 26. The transient begins with a 100°F/hr ramp from 653°F to 191°F. This is followed by a hold at 191°F for a time of 2 hours. Finally, a second 100°F/hr ramp follows from 191°F to 80°F.

- Reactor Trip Thermal Transient

  The reactor trip thermal transient was modeled as three separate ramps as follows: 1) a ramp from 653°F to 613°F over a time of 50 seconds (rate of 2880°F/hr), 2) a second ramp from 613°F to 593°F over a time of 550 seconds (rate of 131°F/hr), and finally 3) a ramp from 593°F back up to 603°F over a time of 233 seconds (rate of 154.5°F/hr). The total analysis transient time is 833 seconds. In the actual transient the temperature reaches 653°F after about 2000 seconds. The cut-off time of 833 seconds is arbitrarily selected so as to be sufficiently long to capture maximum stresses, which typically occur during the steepest part of the transient.

- LOP Transient

  The loss of secondary pressure thermal transient was modeled as an initial downward ramp from 653°F to 353°F in 100 seconds followed by a series of intermediate ramps back up to 528°F, corresponding to a total analysis transient time of 4,000 seconds. The

actual transient goes back up to 653°F after about 8400 seconds. The cut-off time of 4,000 seconds is arbitrarily selected so as to be sufficiently long to capture maximum stresses, which typically occur during the steepest part of the transient.

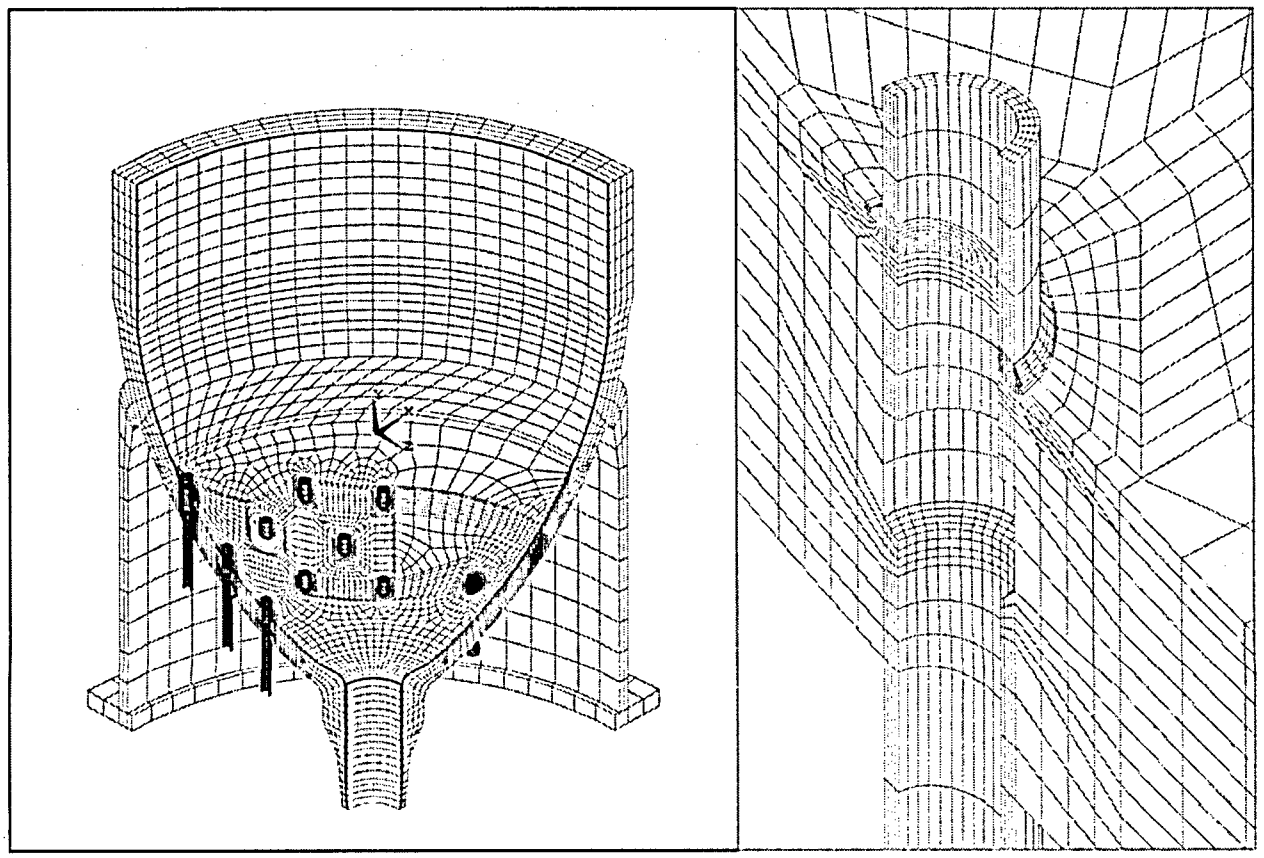

Figure 2-1. Pressurizer Bottom Head Finite Element Model

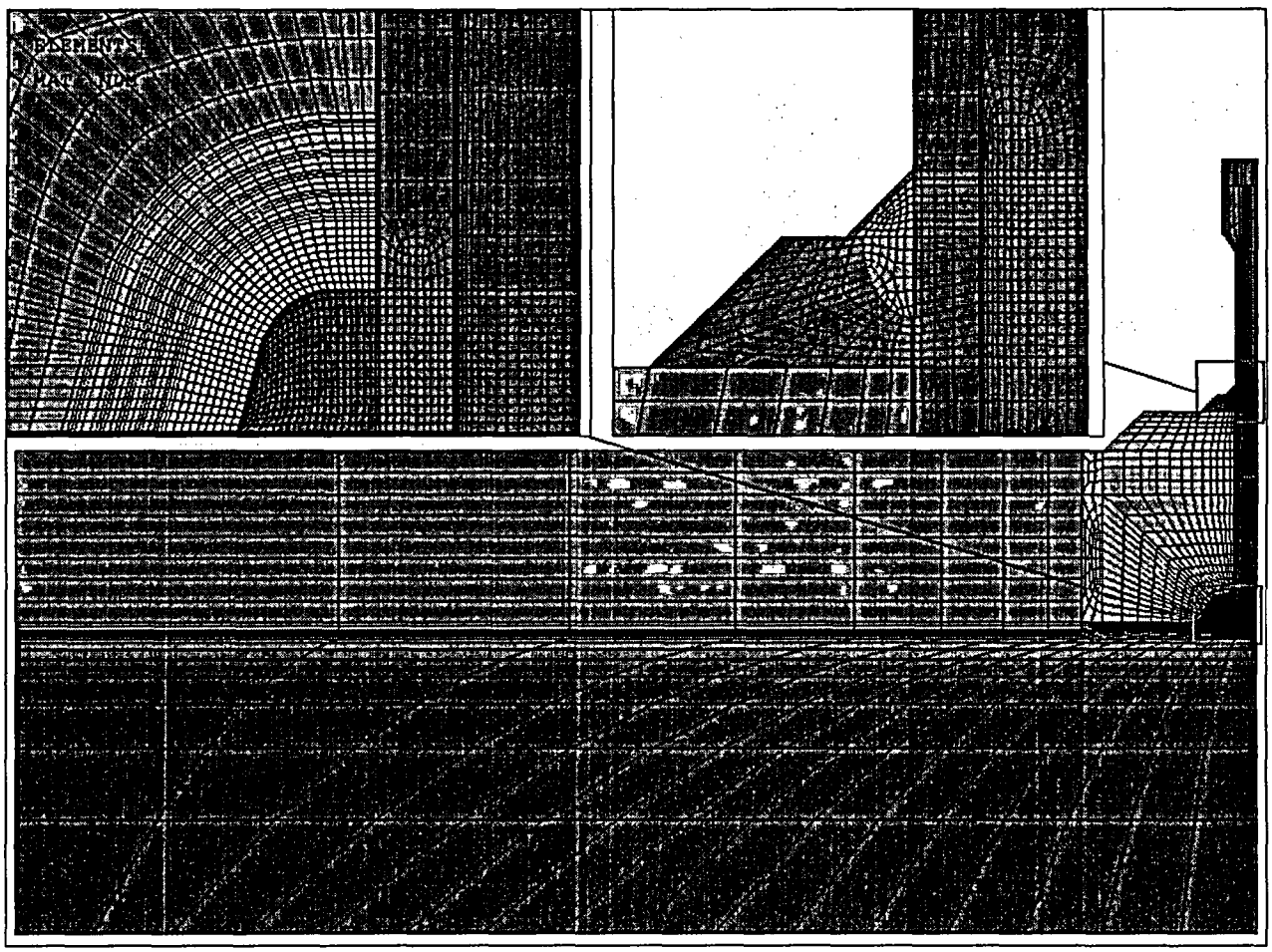

Figure 2-2. Pressurizer Side Shell Temperature Nozzle Finite Element Model

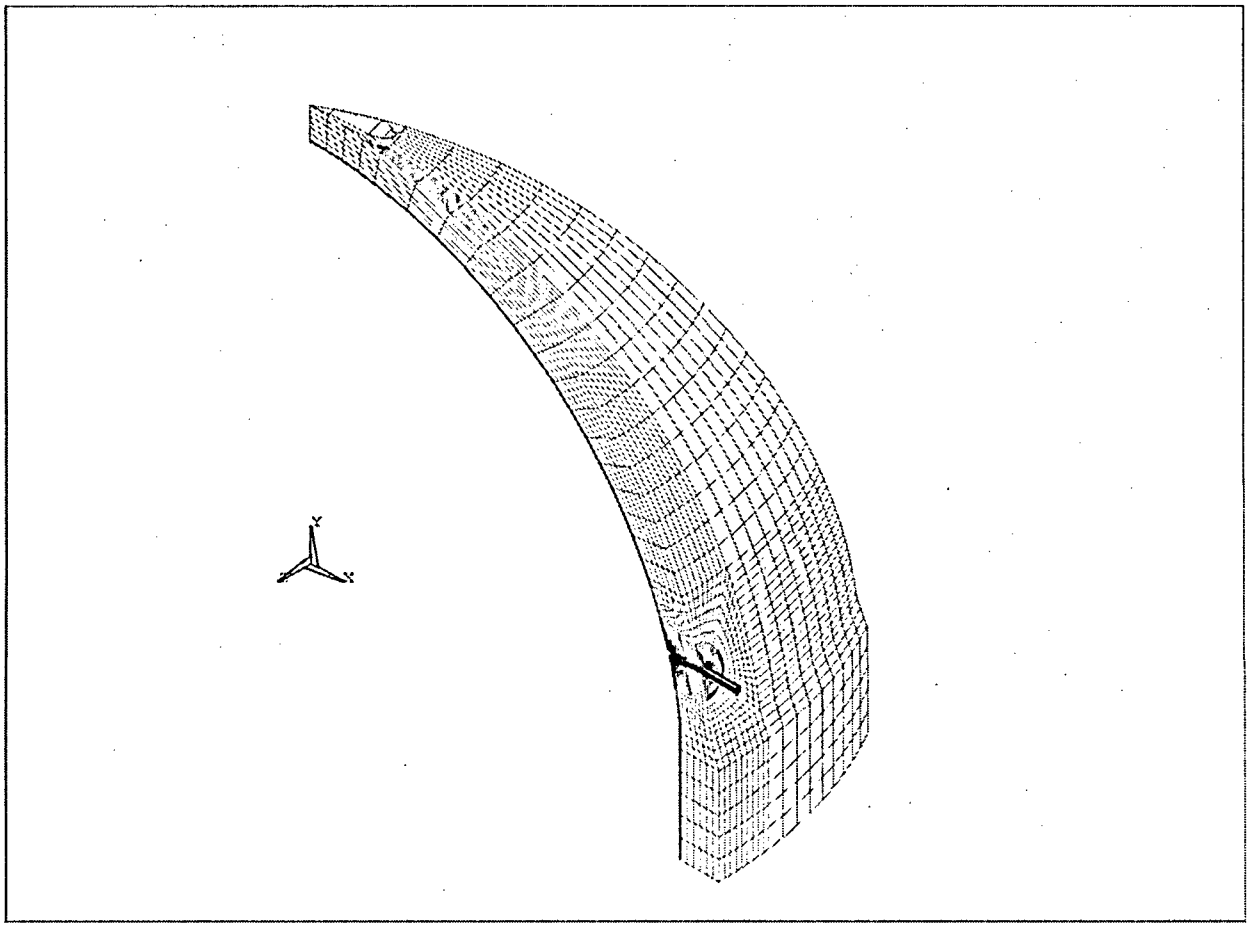

Figure 2-3. Pressurizer Top Head Instrument Nozzle Finite Element Model

3.0 LINEAR ELASTIC FRACTURE MECHANICS

A linear elastic fracture mechanics (LEFM) evaluation by finite element analysis was performed for the pressure small bore nozzles of the pressurizer. For this evaluation, hypothetical flaws were postulated in each of the nozzle penetrations. Then, the stress intensity factors for the postulated flaws in the nozzle penetrations were computed to determine if they meet ASME Code Section XI LEFM requirements. The details of the LEFM evaluations are documented in References 4 and 6 through 8.

3.1 Stress Intensity Factors

The finite element models and the corresponding stress results described in Section 2.0 were used to perform the LEFM evaluation. For the bottom head nozzles, the finite element model used for the stress analysis was modified to include only the nozzle being analyzed, a finer mesh and crack tip elements along the postulated crack front. In order to qualify the repair design for a certain plant operating period by performing a fatigue crack growth evaluation, multiple flaws were postulated for each of the nozzles, with the exception of the top head instrument nozzle, which included only the initial flaw. The initial flaw in each case encompasses the J-groove weld and weld butter such that the flaw front is at the Alloy 600 weld - low alloy steel base metal interface. In addition, for the bottom head heater sleeve and instrument nozzle penetrations, the entire bottom head inside surface cladding is assumed flawed as well. The postulated initial flaws are illustrated in Figures 3-1 through 3-4.

Using the superposition method and the stress results from References 1 through 4 and References 23 to 25, stress intensity factors resulting from residual stresses, internal pressure and the thermal transient events were determined at the postulated crack tips for each of the nozzles, except for the top head instrument nozzle for which the stress intensity factors were computed directly during the stress analyses.

The results of the fracture mechanics analyses were post-processed and the stress intensity factors were determined at multiple locations along the crack fronts. The maximum stress intensity factor results, at any point along the crack front, for a unit pressure (crack face and internal pressure), residual stress, and all applicable thermal transients were extracted along with the time and the corresponding temperature at which they occur for each transient condition. Based on that time, the appropriate scaling factor was applied to the stress intensity factors due to the unit pressure before adding them to those for thermal transient conditions to obtain the maximum total stress intensity factors for each plant event analyzed. The resulting maximum total stress intensity factors are listed in Tables 3-1 through 3-4, for all flaw sizes. In addition, the average total stress intensity factors along the crack front for each of the postulated flaws are shown in Tables 3-1 through 3-4.

3.2 Allowable Stress Intensity Factors

The flaw evaluation criteria of Section XI of the ASME Code [9] define the allowable stress intensity factor under normal operating and upset conditions as the material toughness divided by the safety factor of $\sqrt{10}$. Similarly, the safety factor of $\sqrt{2}$ is prescribed for emergency and faulted plant conditions. The pressurizer bottom head is fabricated from low alloy steel SA-533, Grade B, Class 1. The material fracture toughness (K_{Ia} and K_{Ic}) given in Section XI, Article A-4200 of the ASME Code for low alloy steels, is used to determine the allowable stress intensity factors for all the postulated flaws. The 2005 ASME Pressure Vessels and Piping Division Conference document PVP2005-71718 [10] provides the technical basis for using K_{Ic} in place of K_{Ia}. Therefore, the allowable stress intensity factors are calculated by taking $K_{Ic}/\sqrt{10}$ for normal and upset operating conditions and $K_{Ic}/\sqrt{2}$ for emergency conditions, faulted conditions, and conditions where the internal pressure is less than 20% of the Design Pressure. The critical fracture toughness, K_{Ic}, is calculated based on the temperature at which the maximum stress intensity factor was extracted for each postulated flaw and an RT_{NDT} value of 30°F [11] for the Waterford-3 pressurizer vessel. The calculated allowable stress intensity factors are shown in Tables 3-1 through 3-4 for each of the small bore nozzles for all plant loading conditions analyzed.

3.3 Stress Intensity Factors Comparison

As seen by reviewing the results in Tables 3-1 and 3-2, the ASME Code allowable stress intensity factor criteria are not satisfied for some loading conditions for the pressurizer bottom head heater sleeve and instrument nozzle repairs. Conversely, the results in Tables 3-3 and 3-4 show that all ASME Code allowable stress intensity factor criteria have been met for all loading conditions for the side shell temperature and top head instrument nozzle repairs. Therefore, elastic-plastic fracture mechanics analyses need to be performed for the pressurizer bottom head heater sleeve and instrument nozzle repair designs, but not for the other nozzles.

In the finite element analysis a 100°F/hr instead of a 200°F/hr cooldown rate was used for the top head instrument nozzle. As can be seen in Table 3-4, the calculated maximum stress intensity factor for the cooldown transient is less than half of the ASME Code allowable. Hence, given the large margin, the cooldown rate of 200°F/hr would not impact the conclusions of this evaluation.

It should be noted that the stress intensity factors for end-of-evaluation period flaw sizes due to fatigue crack growth should also be compared to the ASME Code allowable values. For the bottom head nozzles, the stress intensity factors for the as-modeled flaws exceed the Code allowables and, therefore, there is no need to perform any further LEFM comparisons. The end-of-evaluation period stress intensity factor values for the top head instrument nozzle and side shell temperature nozzle will be compared to allowables in Section 5 if the final flaws after the fatigue crack growth exceed the largest modeled flaws.

Table 3-1

LEFM Results – Bottom Head Heater Sleeve Nozzle

Event	Applied Stress Intensity Factor (ksi-$\sqrt{in}$)								Allowable Stress Intensity Factor (ksi-$\sqrt{in}$)	Acceptable?
	Flaw 1		Flaw 2		Flaw 3		Flaw 4			
	Max.	Ave.	Max.	Ave.	Max.	Ave.	Max.	Ave.		
Steady State	89.2	49.0	88.2	56.8	91.5	58.0	107.3	67.3	63.2	No
Heatup (Case A)	3.2	-3.1	3.7	-1.8	9.0	0.9	-1.6	-3.5	141.4	Yes
Heatup (Case B)	31.8	21.4	35.7	26.4	41.6	28.6	72.9	45.5	63.2	No
Heatup (Case C)	31.6	21.7	33.3	25.6	37.4	26.9	60.4	39.2	63.2	Yes
Cooldown (Case A)	180.0	92.4	168.9	103.3	166.0	101.5	138.1	87.4	141.4	No
Cooldown (Case B)	146.5	76.5	141.2	87.4	142.8	88.0	143.1	89.8	63.2	No
Cooldown (Case C)	102.0	54.8	97.5	61.8	97.9	61.3	92.6	58.4	69.3	No
Trip (Case A)	103.8	56.1	101.7	64.6	104.4	65.5	111.1	70.0	63.2	No
Trip (Case B)	115.1	61.5	112.5	70.9	115.2	71.3	126.9	79.4	63.2	No
LOP	185.3	96.1	171.9	106.1	166.2	103.0	118.0	77.2	141.4	No

Table 3-2

LEFM Results – Bottom Head Instrument Nozzle

Event	Applied Stress Intensity Factor (ksi-$\sqrt{in}$)						Allowable Stress Intensity Factor (ksi-$\sqrt{in}$)	Acceptable?
	Flaw 1		Flaw 2		Flaw 3			
	Max.	Ave.	Max.	Ave.	Max.	Ave.		
Steady State	107.6	69.7	103.3	66.0	100.4	70.4	63.2	No
Heatup (Case A)	10.1	4.2	26.0	7.9	26.5	9.3	141.4	Yes
Heatup (Case B)	68.5	43.9	74.9	44.7	74.7	49.3	63.2	No
Heatup (Case C)	82.3	53.1	84.1	51.5	83.1	56.1	63.2	No
Cooldown (Case A)	142.8	92.4	126.8	83.4	118.4	85.0	141.4	No
Cooldown (Case B)	144.3	94.1	130.6	87.3	125.7	91.3	63.2	No
Cooldown (Case C)	128.4	83.5	119.4	78.1	115.4	82.9	63.2	No
Trip (Case A)	113.8	73.8	107.6	69.2	103.8	73.2	63.2	No
Trip (Case B)	126.4	82.3	117.5	76.7	113.6	81.3	63.2	No
LOP	165.9	107.8	143.0	96.7	132.4	96.4	141.4	No

Table 3-3

LEFM Results Summary – Side Shell Temperature Nozzle

Event	Applied Stress Intensity Factor (ksi-$\sqrt{in}$)										Allowable Stress Intensity Factor (ksi-$\sqrt{in}$)	Acceptable?
	Flaw 1		Flaw 2		Flaw 3		Flaw 4		Flaw 5			
	Max.	Ave.	Max.	Ave.	Max.	Ave.	Max.	Ave.	Max.	Ave.		
Steady State	56.6	47.5	54.5	44.9	54.8	45.5	55.5	46.3	56.4	46.4	63.2	Yes
Heatup	38.8	33.3	37.6	31.3	38.6	32.0	40.5	32.8	41.9	33.0	63.2	Yes
Cooldown	27.2	24.2	28.6	24.9	30.7	26.0	32.0	26.8	32.3	26.8	56.1	Yes
Zone 3 HU	24.7	21.4	26.1	20.9	28.2	22.0	30.2	23.1	31.5	23.7	63.2	Yes
Zone 3 CD	55.4	51.1	55.4	50.1	57.3	50.7	58.6	51.4	58.9	50.9	141.4	Yes
Trip	58.0	49.4	56.2	47.5	56.4	48.2	57.1	49.1	57.8	49.2	63.2	Yes
LOP	73.9	66.2	71.1	64.0	72.8	64.4	74.3	64.9	74.6	64.0	141.4	Yes

Table 3-4

LEFM Results Summary – Top Head Instrument Nozzle

Event	Applied Stress Intensity Factor (ksi-$\sqrt{in}$)			Allowable Stress Intensity Factor (ksi-$\sqrt{in}$)	Acceptable?
	Flaw 1		Final Flaw		
	Max.	Ave.	Max.		
Heatup	35.7	29.8	36.3	63.2	Yes
Cooldown	27.3	26.5	27.8	63.3	Yes
Trip	51.0	46.2	51.9	63.2	Yes
LOP	109.3	77.6	NA	141.4	Yes

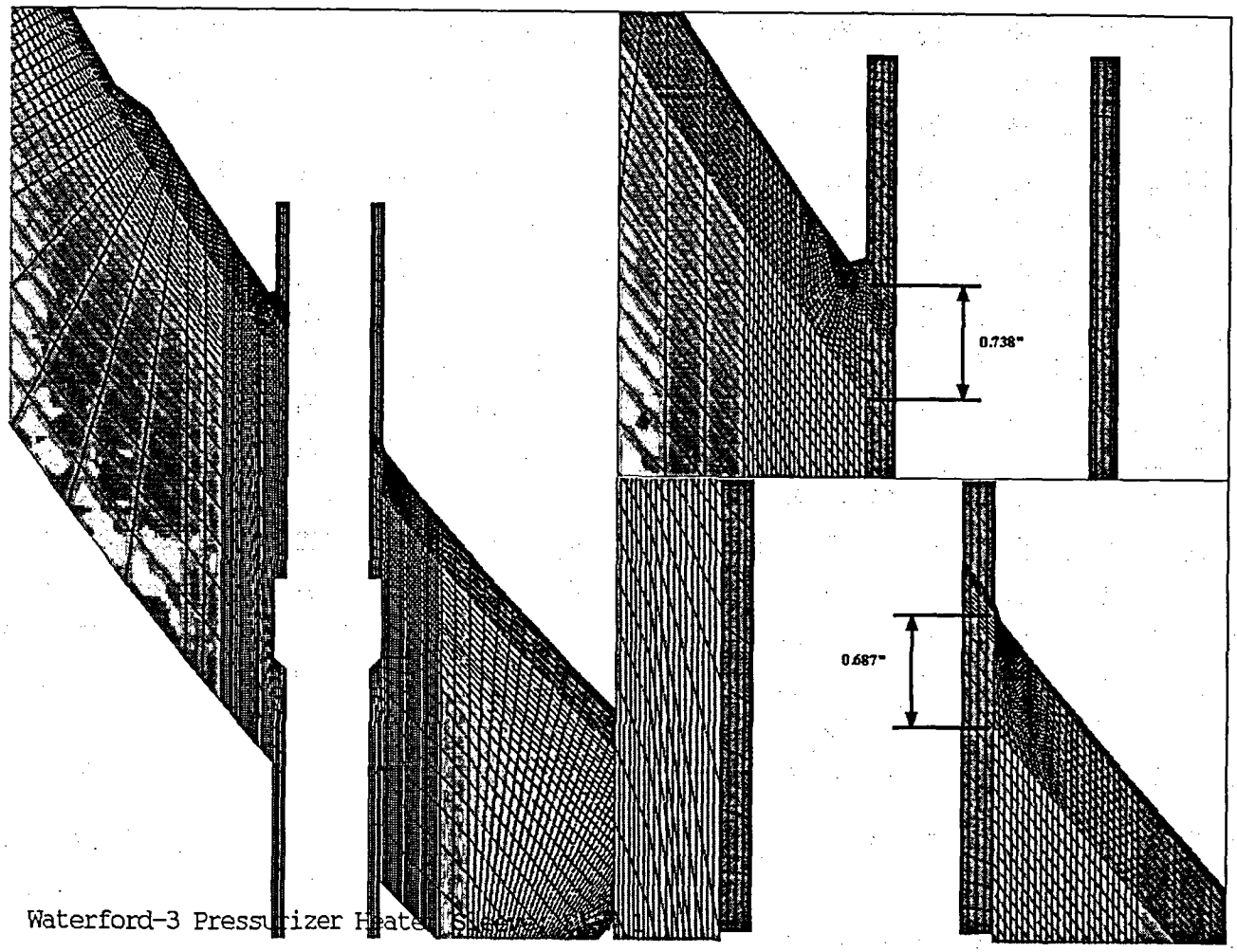

Figure 3-1. Pressurizer Heater Sleeve Nozzle Postulated Flaw Dimensions
(Flawed Portion shown in Magenta) (Flaw 1)

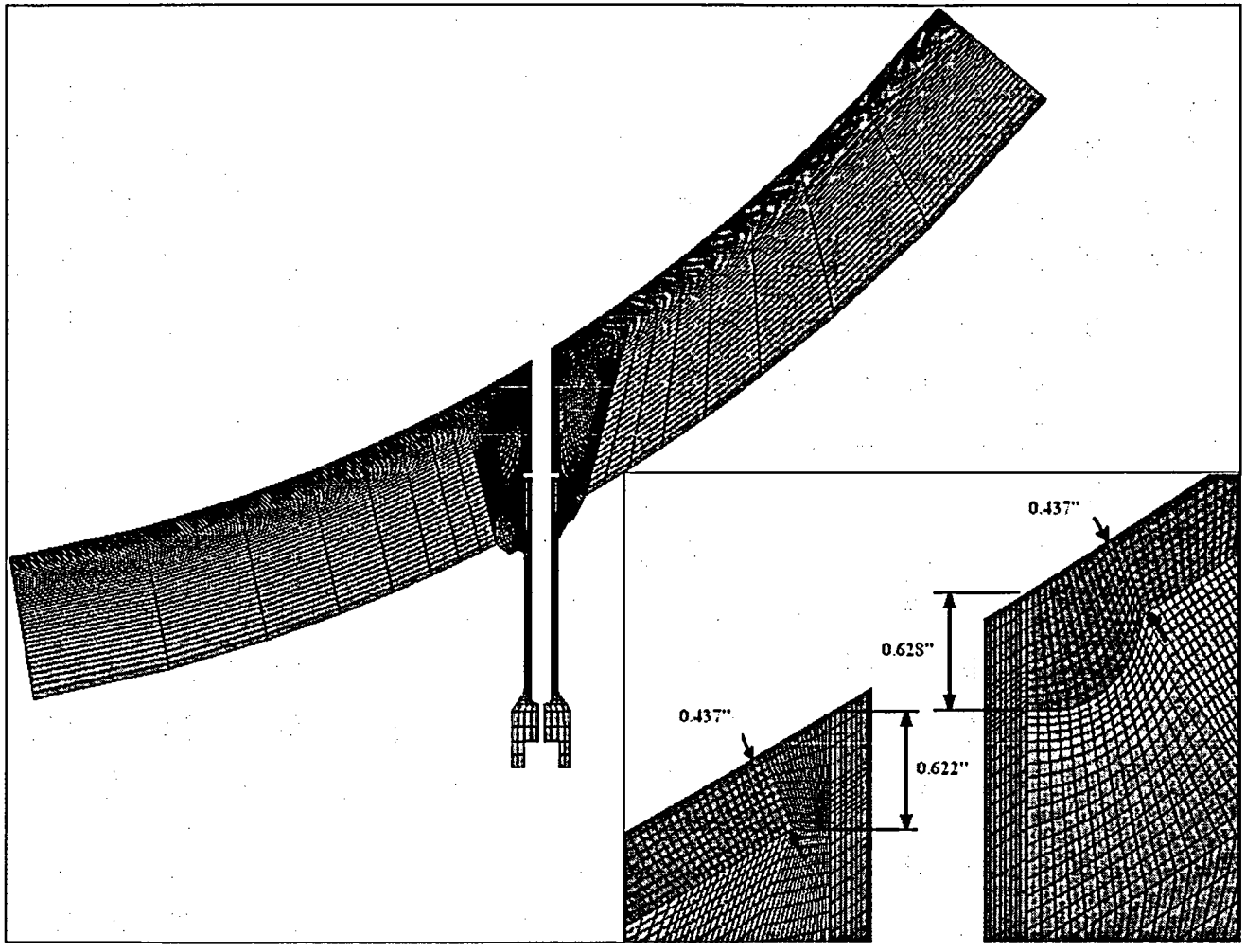

Figure 3-2. Pressurizer Bottom Head Instrument Nozzle Postulated Flaw Dimensions
(Flawed Portion shown in Magenta)

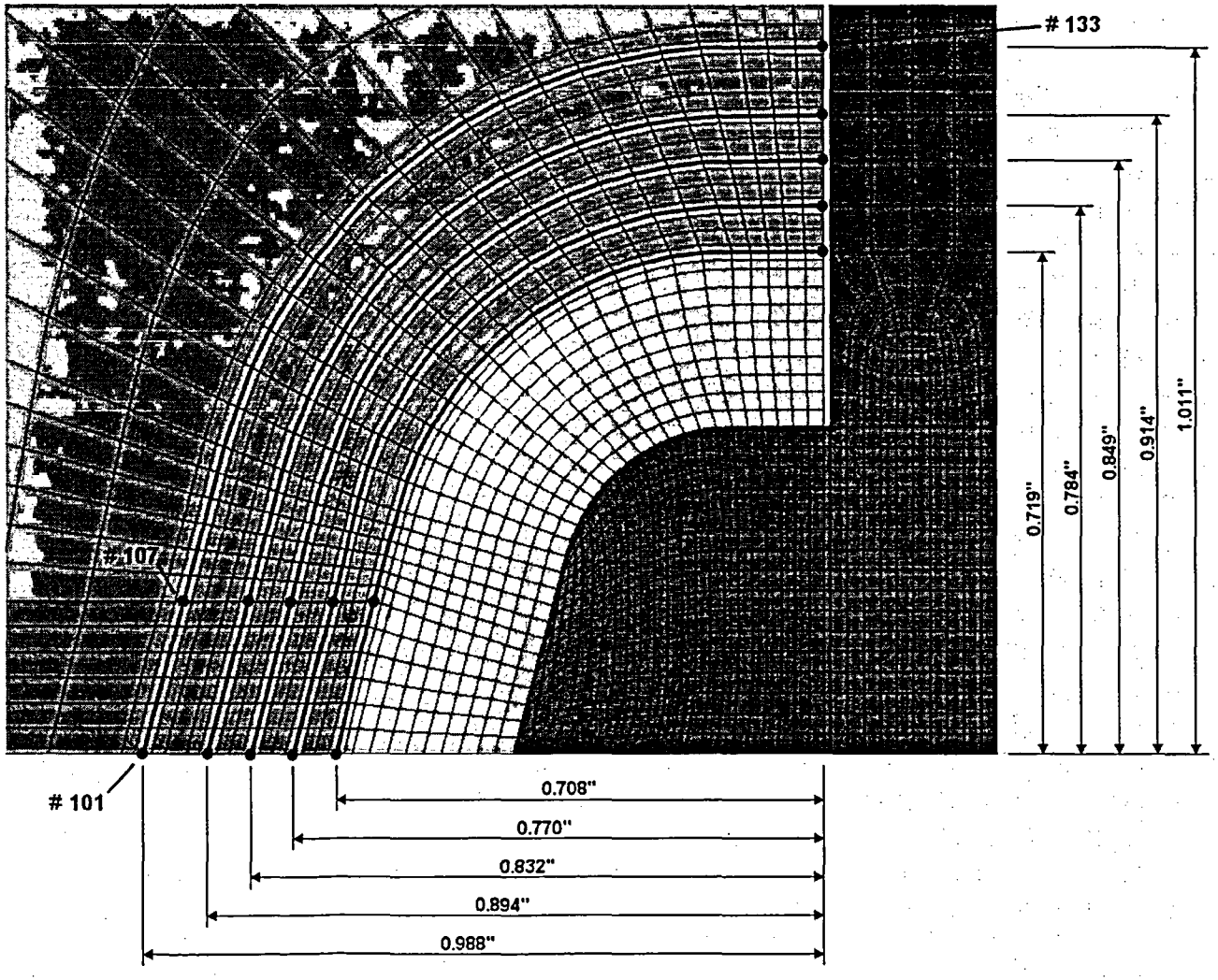

Figure 3-3. Pressurizer Side Shell Temperature Nozzle Flaw Dimensions

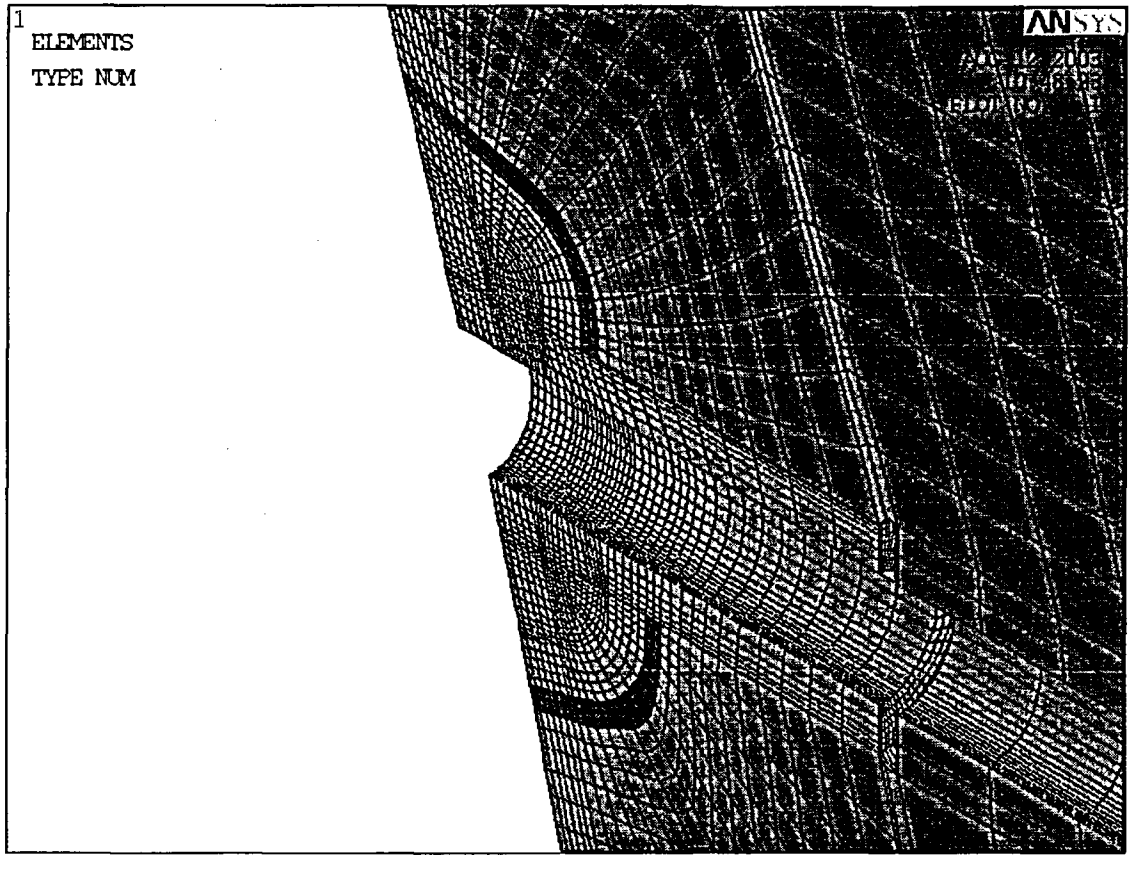

Figure 3-4. Pressurizer Top Head Instrument Nozzle Initial Flaw

4.0 ELASTIC-PLASTIC FRACTURE MECHANICS

In Section 3.0, it was shown that the pressurizer bottom head heater sleeve and instrument nozzles did not satisfy the ASME Code Section XI [9] criteria on a linear elastic fracture mechanics (LEFM) basis. However, the controlling loading conditions in the foregoing LEFM analyses occur at plant operating temperatures for which the low alloy steel pressurizer base material is on the upper shelf of its Charpy V-notch impact energy curve, and therefore possesses considerable ductility. For low alloy steel components in this temperature regime, elastic-plastic fracture mechanics (EPFM) techniques are more appropriate fracture mechanics technologies than LEFM techniques. The LEFM methodology used above treats all loadings on the pressurizer vessel equivalently, applying equal safety factors (~3 for normal and upset loads, and ~1.4 for emergency and faulted loads) to both primary stresses, due to internal pressure and mechanical loads, as well as to secondary and peak stresses, such as those caused by differential thermal expansion and residual stresses. These loadings are equivalent in their potential to produce fracture only in the most brittle of materials, such as glass, RPV beltline materials at low temperatures after significant irradiation embrittlement, and thick, ferritic materials at very low temperatures.

Ample precedent exists in the ASME Code, Section XI for the use of EPFM methodologies in materials that exhibit some ductility. Such precedent may be seen in Appendix C for Evaluation of Flaws in Austenitic Piping [9], Appendix H for Evaluation of Flaws in Ferritic Piping [9], and Appendix K for Assessment of Reactor Vessels with Low Upper Shelf Charpy Impact Energy Levels [9]. Appendix H includes a screening criteria to determine into which regime a ferritic piping flaw evaluation falls (LEFM, EPFM or Limit Load), and for problems that fall into the EPFM regime, specifies different safety factors for primary stresses (SF=3) than for secondary loadings (SF=1). An even more appropriate approach for the pressurizer heater sleeve and instrument nozzle penetrations is presented in Appendix K [9]. In addition to different safety factors for primary versus secondary loadings, this appendix also provides a procedure for performing flaw instability analysis of reactor vessel materials on the upper shelf, as illustrated schematically in Figure 4-1. The left hand plot in this figure illustrates a typical material

J-Resistance (J-R) curve. As loading is applied to the top of a fracture specimen of a ductile material, the J value for that material increases until it exceeds the material fracture toughness, J_{Ic} (similar to K_{Ic} in LEFM evaluations). At this point, if the material is ductile, the crack in the specimen will begin to extend in a slow stable fashion until it reaches the instability point indicated by the upper extent of the J-R curve. For analytical convenience, the material J-R curve may be converted to J versus Tearing Modulus (T), as illustrated in the right hand plot in Figure 4-1. Application of this Tearing Modulus to an engineering component, such as the Waterford-3 pressurizer, is then performed by computing J versus T applied for the component, illustrated by the dashed line on the right hand plot. The J-value at which the J-applied line crosses J_{Ic} corresponds to the initiation of slow stable crack propagation. Unstable crack propagation or failure, however, is not predicted until the instability point in the diagram is reached. The difference between $J = J_{Ic}$ versus J at the instability point is a measure of the additional ability to sustain loading afforded by the ductility of the material. In a brittle material, failure occurs at $J = J_{Ic}$ (equivalent to $K = K_{Ic}$ in an LEFM analysis).

In this section, the technical approach and approximate methodology of Appendix K [9] is applied to the Waterford-3 pressurizer postulated remnant crack under the controlling plant event for each of the bottom head nozzles. Safety factors of 3.0 for primary loads and 1.5 for secondary loads are applied, which are more conservative than those required by Appendices C, H or K. The details of the EPFM evaluation are documented in References 12 and 13.

4.1 Material J-Resistance Curve

Appendix K [9] specifies three methods for selection of the material J-integral resistance curve. A J-R curve may be generated by actual testing of the material following accepted test procedures, it may be generated from a J-integral database obtained from the same class of material with the same orientation, or an indirect method of estimating the J-R curve may be used, provided the method is justified for the material. For this analysis, an indirect method is used, based on Charpy V-notch correlations contained in Reference 14.

Figure 4-2, obtained from Reference 14, presents J-T materials curves for irradiated and unirradiated nuclear vessel steels at various upper shelf Charpy V-notch energy levels (in joules). The results show a rough correlation, in that higher J-T curves are generally obtained for higher Charpy V-notch energy levels. An actual correlation curve has been developed (Figure 4-3 and Figure 4-4) between Charpy V-notch energy and the parameters of a J-R curve power law fit of the following form:

$$J = C\,(\Delta a)^m$$

In general, a power law fit of this type is only valid for small crack extension (Δa). However, Loss and coworkers [15] have observed good fit for the power law for larger Δa for materials with high upper shelf Charpy energy levels, such as those addressed herein.

Only three Charpy V-notch data points were available for the Waterford-3 pressurizer bottom head plate M2610-2. The data points were at +10°F with energies of 44 ft-lbs, 35 ft-lbs and 34 ft-lbs [11]. The bottom head plate is made from SA-533 Grade B, Class 1 material. Additional data from the Waterford-3 vessel beltline surveillance plate contains a full Charpy V-notch data set in the unirradiated condition for the plate M-1004-2 [16]. This material is also a SA-533 Grade B, Class 1 ferritic steel of the same vintage as the pressurizer bottom head plate. These materials were assumed to be similar for the purpose of this evaluation, i.e., the vessel shell plate properties are representative of the pressurizer bottom head plate.

A least-squares curve-fit to the Waterford-3 Charpy surveillance plate data was performed. The transverse Charpy V-notch fitted mean curve and data are shown in Figure 4-5. For comparison, the pressurizer bottom head Charpy data points are superimposed on this plot. The pressurizer bottom head plate data are within the range of scatter of the vessel plate data. A statistical regression analysis was performed for hyperbolic tangent curve-fits to Charpy V-notch data including Waterford-3 plate surveillance data and a limited set of pressurizer bottom head plate data. The similarity of the materials are such that they were combined to yield a statistical fit for the projected upper shelf Charpy energy using a 95% lower bound

prediction limit to the asymptotic upper shelf. The 95% lower bound prediction limit for the combined fitted results produces an upper shelf energy of 118 ft-lbs. By comparison, a lower bound 95% confidence limit for upper shelf energy based on the fitted results would be approximately 132 ft-lbs. Therefore, the estimated value for upper shelf energy of 118 ft-lbs was used in the EPFM evaluation for the Waterford-3 pressurizer bottom head nozzle penetrations.

Based on this CVN of 118 ft-lbs and a reference flow stress of 85 ksi, Figure 4-3 and Figure 4-4 are used to determine values of the coefficient "C" and the exponent "m" for the power law J-R curve. These have been converted to a J-T diagram, and are illustrated by the "118 ft-lb" J-T curve in Figure 4-6 and Figure 4-7 for the bottom head heater sleeve nozzle at the uphill and downhill locations, respectively (Final flaw size shown). Similarly, the J-T diagrams for the bottom head instrument nozzle are shown in Figures 4-8 and 4-9 for uphill and downhill locations, respectively.

4.2 Calculation of Applied J-T

Analyses for J-T applied were performed in accordance with the approximate technique of ASME Code, Section XI, Appendix K [9]. The EPFM J-integral estimates were developed from the foregoing LEFM stress intensity factor calculations. The Appendix K approximate procedure for J-integral involves the calculation of a plastic zone corrected crack size for small scale yielding from elastically calculated K values, in accordance with the following:

$$a_e = a + [1/(6\pi)]\ [\ (K_{Ip} + K_{It})/YS]^2$$

The J-integral is then calculated from revised stress intensity factors (K'_{Ip} and K'_{It}) computed at the plastic zone corrected crack size as follows:

$$J = (K'_{Ip} + K'_{Ir})^2/E'$$

The controlling loading condition is determined for each of the nozzle penetrations being evaluated. Taking into account the safety factors of 3.0 and 1.5 on primary and secondary loads, respectively, it was determined that the bounding load condition is the high pressure Cooldown case (Case B) for both bottom head nozzle penetrations. The corresponding stress intensity factor distributions were used to determine the equation for the relationship of K_I with increasing crack size.

4.3 Results of EPFM Analysis

A list of plastic zone size adjusted K' and associated J-applied values, computed in accordance with the above described method is provided in Table 4-1 and Table 4-2 for the initial and final flaw sizes at both the uphill and downhill locations for the heater sleeve nozzle and instrument nozzle, respectively. Results are reported without and with the safety factors of 3.0 on primary loads and 1.5 on secondary loads, as indicated in the second column of the tables. The results are plotted as the J-T applied lines in Figure 4-6 and Figure 4-7 for the bottom head heater sleeve nozzle penetration at the uphill and downhill side, respectively. Likewise, the J-T Applied line is plotted in Figure 4-8 and Figure 4-9 for the bottom head instrument nozzle penetration at the uphill and downhill side, respectively. For each plot, data points are indicated on the J-T Applied line with the corresponding values of safety factors denoted.

The final end of evaluation period flaw sizes from the fatigue crack growth analyses performed in References 17 and 18 exceed the final as-modeled flaws in some cases, for the bottom head nozzles. Specifically, the flaws are exceeded for both the uphill and downhill flaws of the bottom head instrument nozzle, and at the downhill flaw for the heater sleeve nozzle. Therefore, the stress intensity factors are extrapolated for the end-of-evaluation period flaw sizes computed in the fatigue crack growth analyses, and are qualified by EPFM analysis. The results are included in Table 4-1 and Table 4-2, and are plotted in Figure 4-10 for the heater sleeve nozzle, and in Figure 4-11 and Figure 4-12 for the bottom head instrument nozzle.

As discussed above, the appropriate safety factors for normal/upset operating conditions for ductile materials are SF=3 on primary and SF=1.5 on secondary. For both the bottom head heater sleeve nozzle and the bottom head instrument nozzle, it is seen that the applied J for both the initial and final flaw sizes are below the instability limit by a large margin. Therefore, it can be stated that the ASME Code, Section XI allowable flaw size for each of the bottom head nozzles is even greater than the postulated final flaw size.

Table 4-1

J-T Instability Computations – Heater Sleeve Nozzle

Flaw	Safety Factors	K_{Ip}	K_{It}	K_{total}	r_p	a_e	K'_{Ip}	K'_{It}	K'_{total}	J'total	T' (1)	J @ Instability (2)
		(ksi-in$^{1/2}$)			(in)		(ksi-in$^{1/2}$)			(in-kips/in^2)		(in-kips/in^2)
UPHILL												
Initial (Flaw 1)	SF=1	18.0	40.4	58.4	0.087	0.526	18.4	40.2	58.7	0.112	0.988	3.62
	SF=3, 1.5	54.0	60.6	114.6	0.336	0.775	61.9	54.4	116.2	0.439	3.877	3.62
Final (Flaw 4)	SF=1	28.1	21.9	50.0	0.064	1.685	28.6	21.6	50.2	0.082	0.196	6.72
	SF=3, 1.5	84.3	32.9	117.2	0.352	1.973	93.5	25.5	118.9	0.460	1.099	6.72
DOWNHILL												
Initial (Flaw 1)	SF=1	25.9	50.4	76.3	0.149	0.587	30.9	52.2	83.1	0.224	1.985	3.62
	SF=3, 1.5	77.7	75.6	153.3	0.602	1.040	117.2	70.6	187.8	1.147	10.147	3.62
Final (Flaw 4)	SF=1	51.2	38.3	89.5	0.205	1.947	55.5	36.8	92.3	0.277	0.616	6.95
	SF=3, 1.5	153.6	57.4	211.0	1.141	2.883	217.1	39.4	256.5	2.138	4.755	6.95
Final (45 years FCG)(3)	SF=1	67.6	29.2	96.8	0.240	2.861	72.0	26.5	98.5	0.315	0.466	8.41
	SF=3, 1.5	202.9	43.8	246.7	1.560	4.181	287.4	17.4	304.8	3.019	4.464	8.41

Notes:

(1) $T' = \left(\frac{K'total}{\sigma_f}\right)^2 \times \left(\frac{1-\mu^2}{a_i}\right)$, where $\mu = 0.3$, and a_i = initial flaw depth (Flaw 1 or Flaw 4).

(2) J @ instability is defined as J at the intersection of the applied J-T line (J'total vs. T') and the J-T material curve (J vs. T).

(3) Final crack size of 2.621 inches is analyzed, in accordance with the fatigue crack growth evaluation for 45 years of operation [18]. Stress intensity factors are extrapolated for the given crack size.

Table 4-2

J-T Instability Computations – Bottom Head Instrument Nozzle

Flaw	Safety Factors	K_{Ip}	K_{It}	K_{total}	r_p	a_e	K'_{Ip}	K'_{It}	K'_{total}	J'total	T' (1)	J @ Instability (2)
		(ksi-in$^{1/2}$)			(in)		(ksi-in$^{1/2}$)			(in-kips/in^2)		(in-kips/in^2)
UPHILL												
Initial (Flaw 1)	SF=1	22.1	50.8	72.9	0.136	0.574	25.6	56.1	81.7	0.217	1.920	3.61
	SF=3, 1.5	66.2	76.3	142.5	0.520	0.958	98.5	89.8	188.2	1.152	10.190	3.61
Final (Flaw 3)	SF=1	31.5	59.6	91.1	0.213	1.093	35.2	60.3	95.4	0.296	1.303	5.02
	SF=3, 1.5	94.4	89.4	183.8	0.866	1.746	139.4	93.5	232.9	1.763	7.763	5.02
Final (45 years FCG)(3)	SF=1	40.3	61.2	101.4	0.264	1.651	44.8	62.0	106.8	0.371	1.037	6.24
	SF=3, 1.5	120.8	91.8	212.6	1.158	2.545	180.9	97.3	278.2	2.515	7.027	6.24
DOWNHILL												
Initial (Flaw 1)	SF=1	29.4	64.4	93.9	0.226	0.668	31.0	55.5	86.5	0.243	2.131	3.64
	SF=3, 1.5	88.3	96.7	185.0	0.877	1.319	124.8	60.3	185.1	1.114	9.766	3.64
Final (Flaw 3)	SF=1	33.1	52.4	85.5	0.188	0.986	36.2	48.0	84.2	0.230	1.119	4.80
	SF=3, 1.5	99.4	78.6	178.0	0.812	1.610	139.1	50.0	189.1	1.162	5.645	4.80
Final (45 years FCG)(3)	SF=1	44.1	36.6	80.7	0.167	1.639	46.8	32.7	79.5	0.205	0.541	6.42
	SF=3, 1.5	132.3	54.9	187.2	0.898	2.370	176.3	23.3	199.5	1.294	3.406	6.42

Notes:

(1) $T' = \left(\frac{K'total}{\sigma_f}\right)^2 \times \left(\frac{1-\mu^2}{a_i}\right)$, where $\mu = 0.3$, and a_i = initial flaw depth (Flaw 1 or Flaw 3).

(2) J @ instability is defined as J at the intersection of the applied J-T line (J'total vs. T') and the J-T material curve (J vs. T).

(3) Final crack sizes of 1.387 inches at the uphill location and 1.472 inches at the downhill location are analyzed, in accordance with the final crack sizes evaluated in the fatigue crack growth evaluation for 45 years of operation [17]. Stress intensity factors are extrapolated for the given crack sizes.

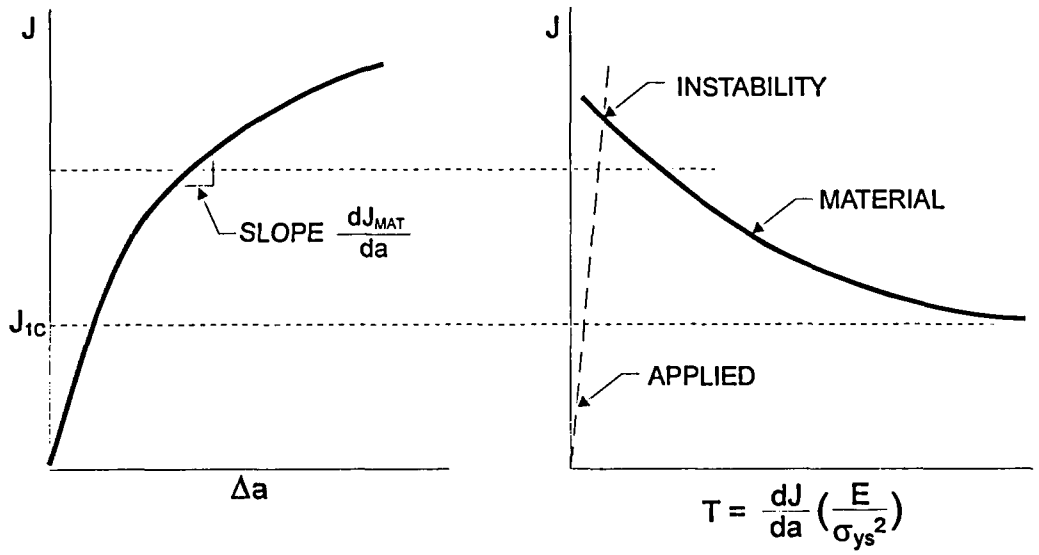

93220r0

Figure 4-1. Schematic of EPFM Stability Analysis from ASME Code, Section XI, Appendix K

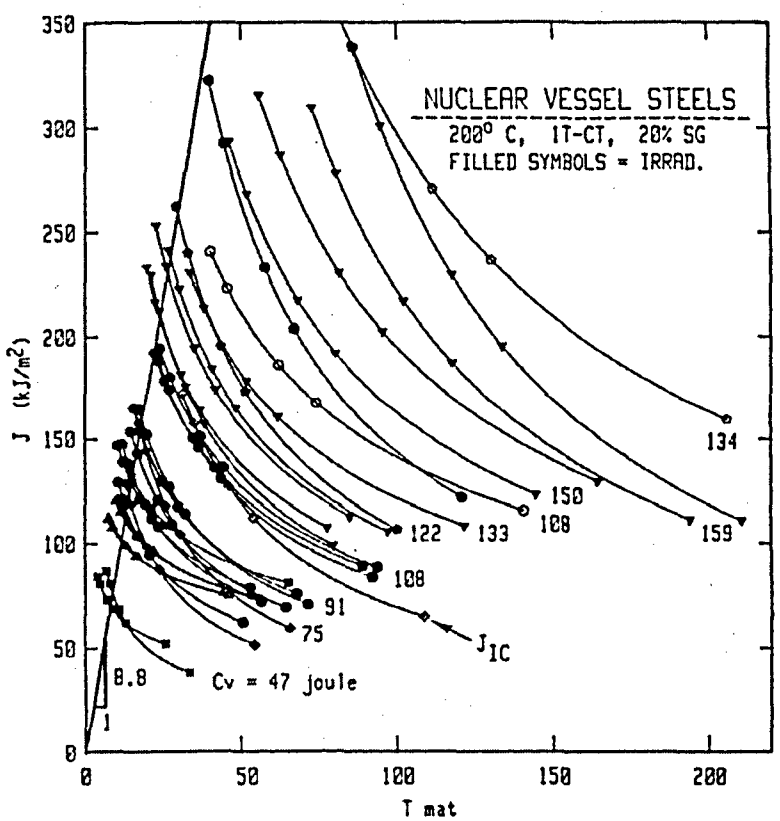

Figure 4-2. J-T Diagram for Several Reactor Vessel Steels and Welds Showing Rough Correlation with Charpy V-notch Upper Shelf Energy

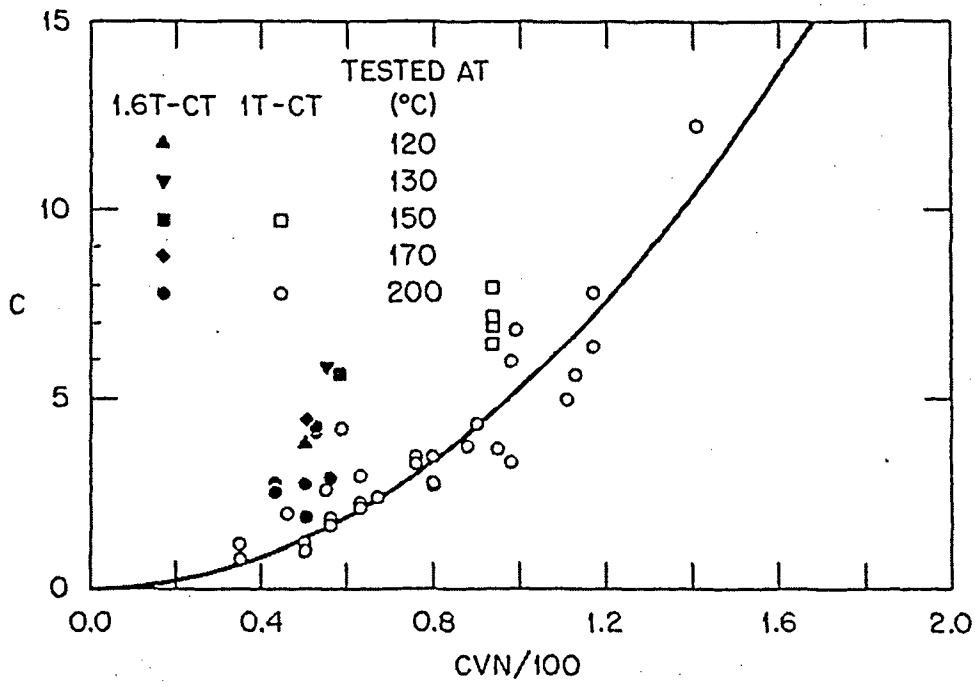

Figure 4-3. Correlation of Coefficient C of Power Law J-R Curve Representation with Charpy V-notch Upper Shelf Energy

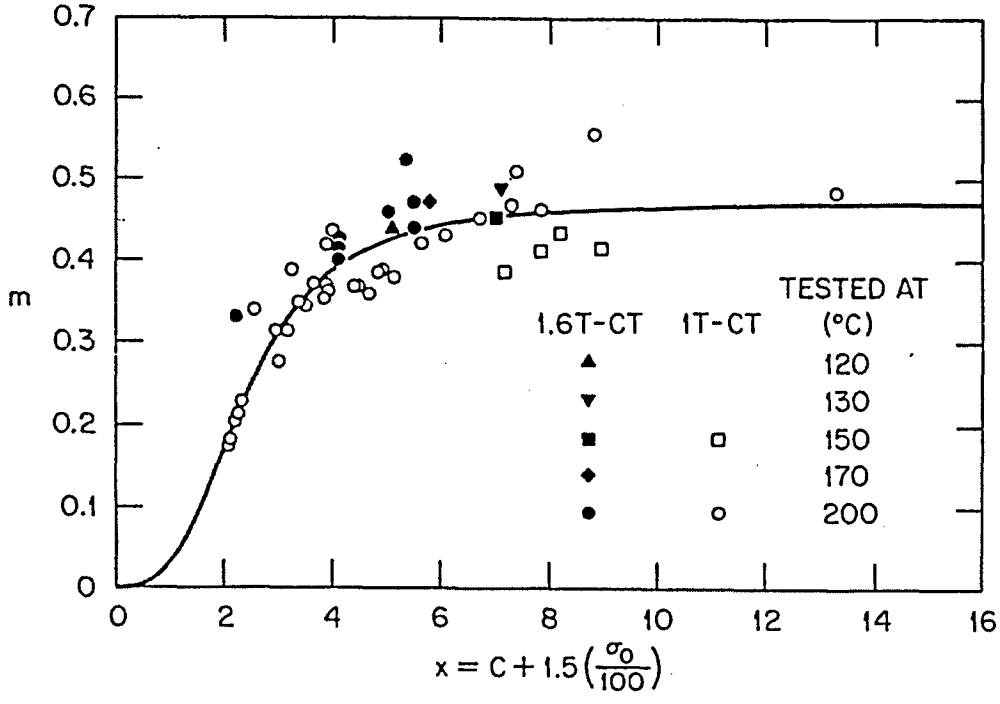

Figure 4-4. Correlation of Exponent m of Power Law J-R Curve Representation with Coefficient C and Flow Stress σ_o

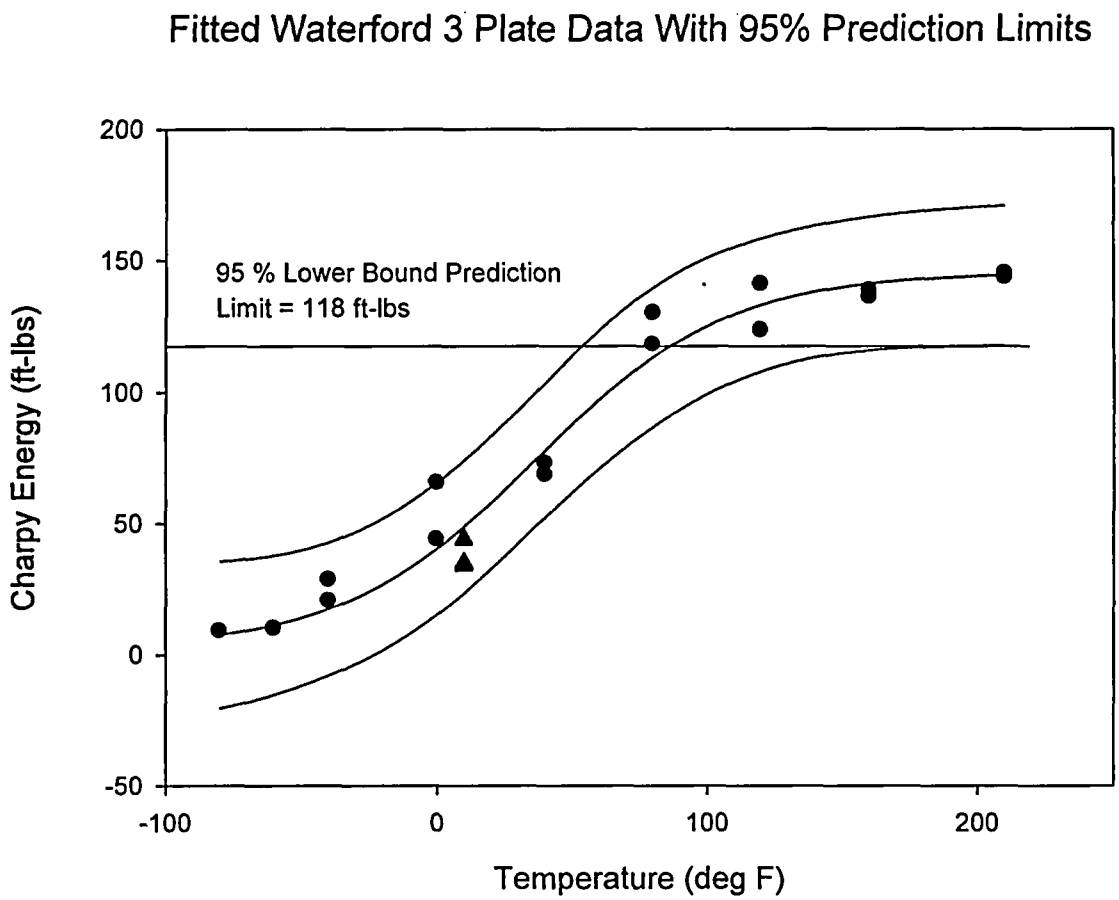

Figure 4-5. Fitted Charpy V-notch Data for Waterford-3 Vessel Surveillance Plate and Pressurizer Bottom Head Plate Showing 95% Prediction Limits

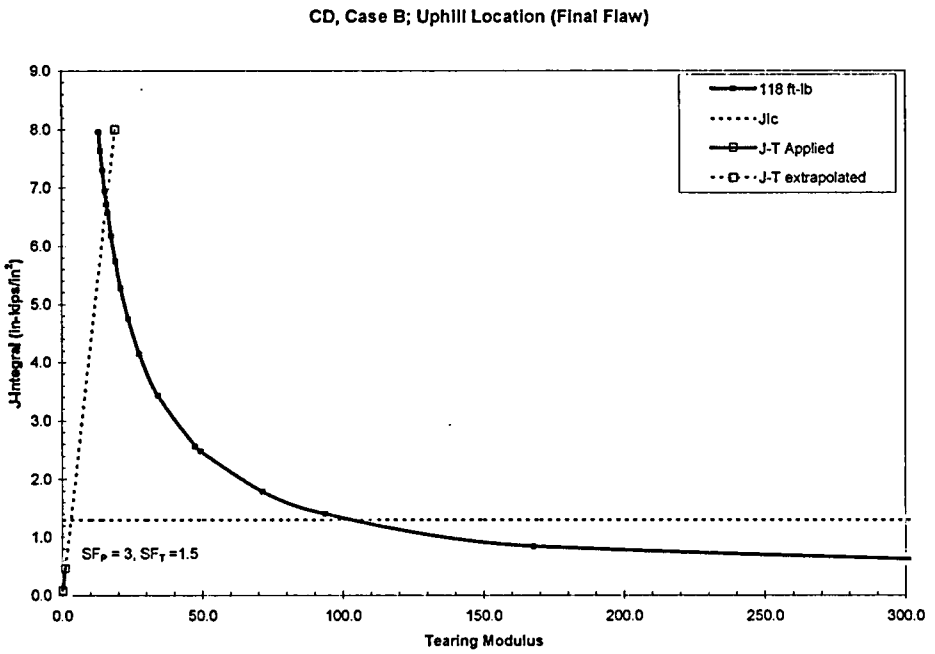

Figure 4-6. J-T Diagram for EPFM Stability Analysis – Heater Sleeve Nozzle Penetration at Uphill Location, Largest Modeled Flaw

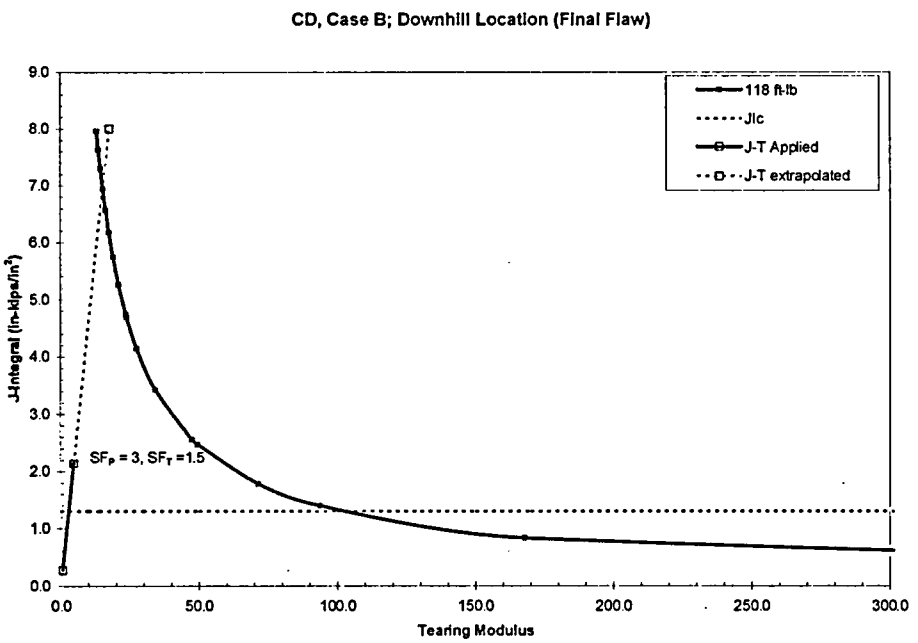

Figure 4-7. J-T Diagram for EPFM Stability Analysis – Heater Sleeve Nozzle Penetration at Downhill Location, Largest Modeled Flaw

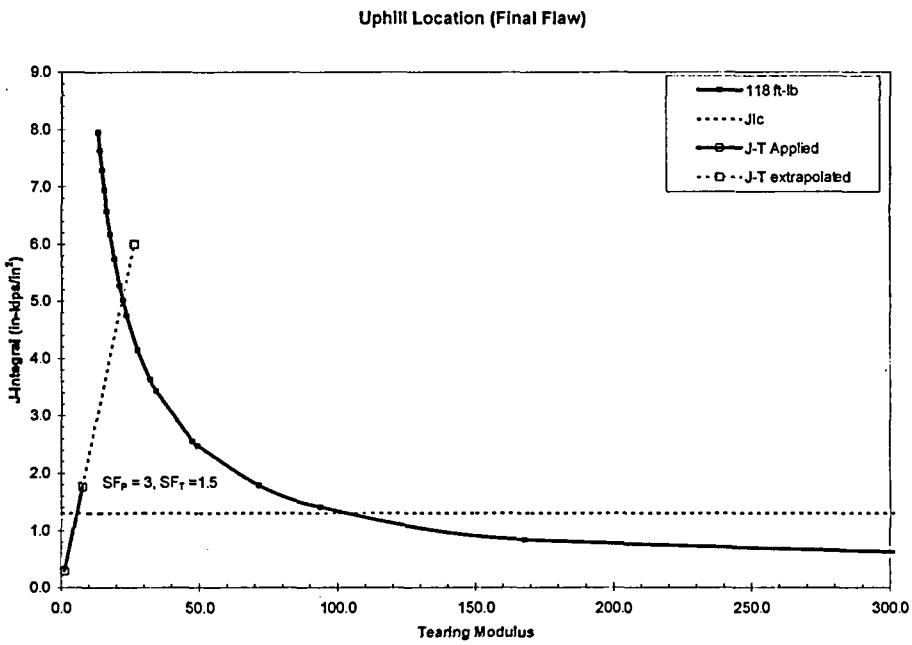

Figure 4-8. J-T Diagram for EPFM Stability Analysis – Bottom Head Instrument Nozzle at Uphill Location, Largest Modeled Flaw

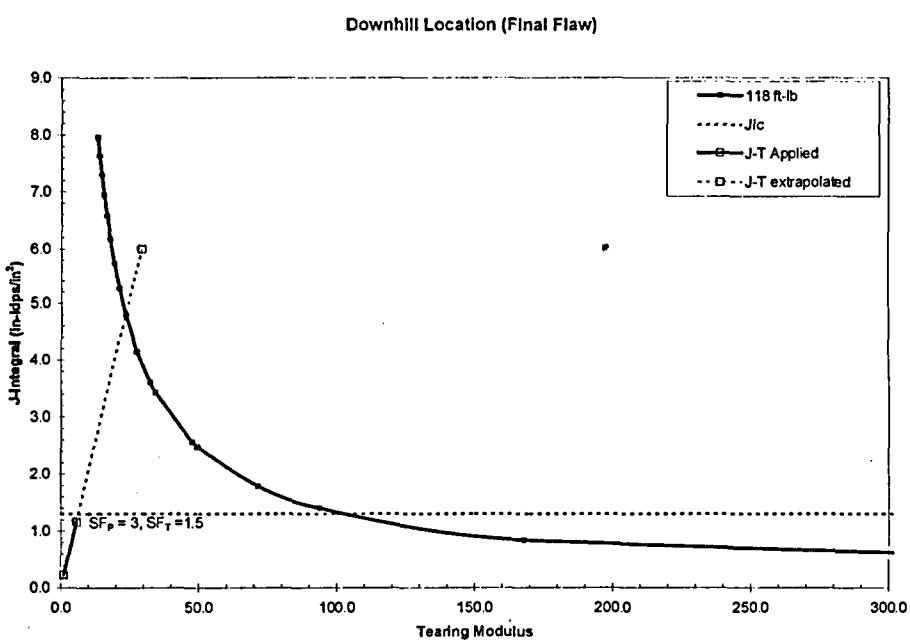

Figure 4-9. J-T Diagram for EPFM Stability Analysis – Bottom Head Instrument Nozzle at Downhill Location, Largest Modeled Flaw

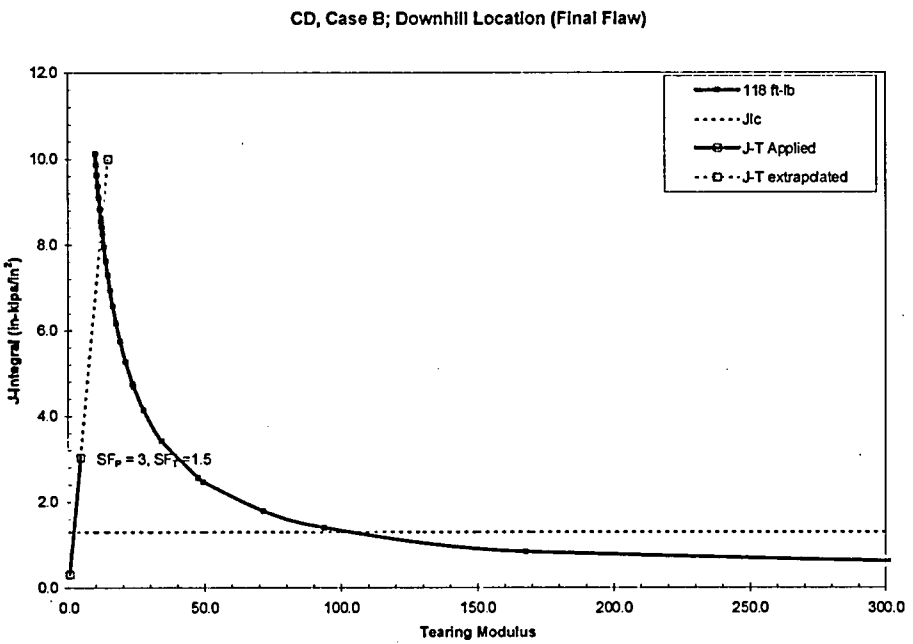

Figure 4-10. J-T Diagram for EPFM Stability Analysis – Heater Sleeve Nozzle Penetration at Downhill Location, End of Evaluation Period Flaw

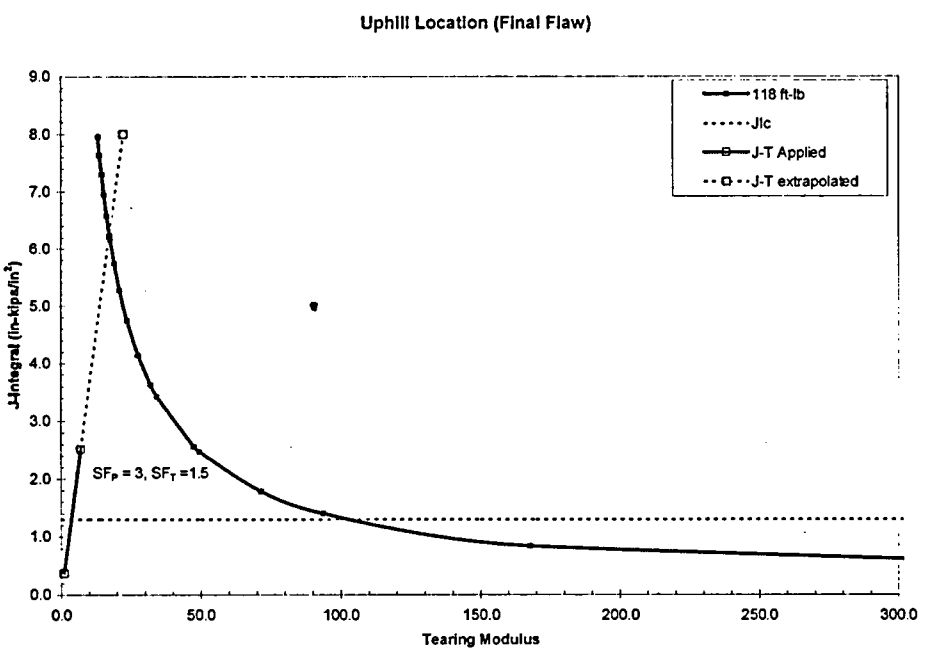

Figure 4-11. J-T Diagram for EPFM Stability Analysis – Bottom Head Instrument Nozzle at Uphill Location, End of Evaluation Period Flaw

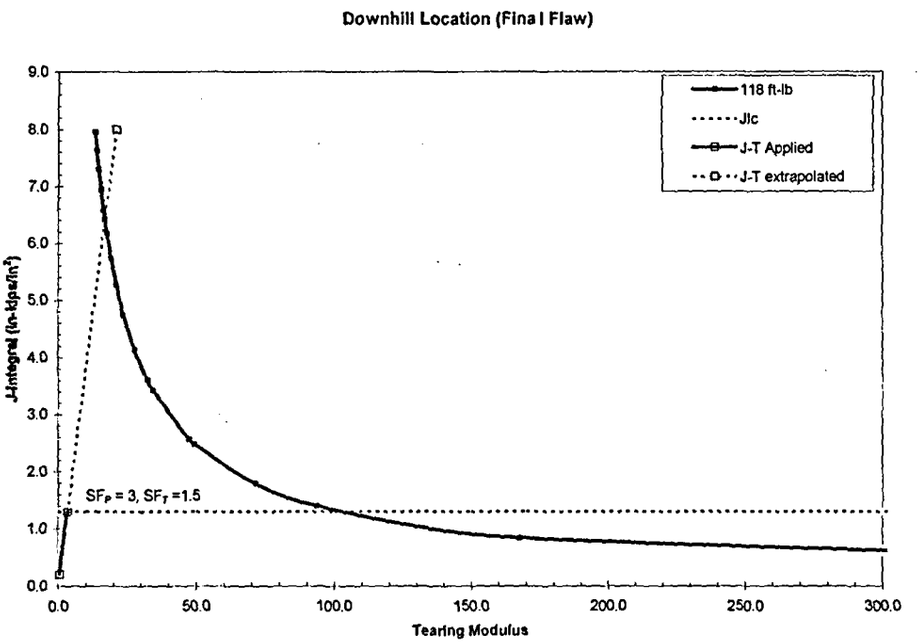

Figure 4-12. J-T Diagram for EPFM Stability Analysis – Bottom Head Instrument Nozzle at Downhill Location, End of Evaluation Period Flaw

5.0 FATIGUE CRACK GROWTH ANALYSIS

In order to qualify the repair design for operation for a certain period, a fatigue crack growth evaluation of the Waterford-3 pressurizer small bore nozzle penetrations was performed. The details of the fatigue crack growth evaluation are documented in References 17 through 20.

5.1 Fatigue Cycle Definition

The Waterford-3 plant operation design transients are specified in References 5 and 21. A list of the design transients is presented in Table 5-1 for the bottom head nozzles. Tables 5-2 and 5-3 present the list of plant transients used in the evaluation of the pressurizer side shell temperature nozzle and top head instrument nozzle, respectively. The loss of secondary pressure transient a faulted condition transient, is not included in this evaluation. The specified number of design cycles for each of the analyzed plant transients over a 40-year time interval is also listed in Tables 5-1 through 5-3. The total number of design cycles of each transient is divided by 40 in order to obtain the approximate number of cycles that occurs per year. The analyses used the number of yearly cycles to calculate the crack growth over a 45-year period for each of the pressurizer small bore nozzles under consideration.

In the crack growth analyses, the design transient cycles are assumed to be evenly distributed over the 45-year interval. Based on the stress intensity factor values, load pairings expected to provide the most conservative results were defined. The defined cyclic load ranges and corresponding number of cycles are presented in Table 5-1 through 5-3.

5.2 Postulated Flaws

For the fatigue crack growth evaluation, multiple flaws were postulated for each of the nozzles, except for the top head instrument nozzle that included only the initial flaw. As illustrated in Figures 3-1 through 3-4, the initial flaw in each case encompasses the J-groove weld and weld butter such that the flaw front is at the Alloy 600 weld - low alloy steel base metal interface. In

addition, for the bottom head nozzle penetrations, the entire inside surface cladding is assumed flawed as well. To simulate crack growth, the postulated flaws in the J-groove weld and cladding are assumed to grow in a self-similar manner into the low alloy steel base metal.

5.3 Stress Intensity Factor Distribution

In order to perform the crack growth analysis, the relationship between the stress intensity factor and the crack size needs to be determined. The stress intensity factors computed for the different postulated flaws for each of the nozzles are presented in Section 3.0. However, for the top head instrument nozzle, the stress intensity factors were only calculated for the initial flaw size. Therefore, the following approximation was used to determine the "K" versus "a" distribution for each transient based on the calculated initial stress intensity factors (K_{Ii}) at the initial flaw size (a_i):

$$K_I = K_{Ii}\sqrt{\frac{a}{a_i}}$$

This approximation, which is based on the assumption that the stress intensity factor (K) is proportional to the square root of the flaw size (a), is conservative since the dominant stresses tend to decrease rather than increase when the crack size becomes larger.

5.4 Fatigue Crack Growth Law

The postulated flaws can potentially grow due to cyclic fatigue loading. For the flaw growth through the pressurizer shell, it was assumed that base material fatigue is the primary propagation mechanism. The methodology of Section XI of the ASME Code [9] was used to perform the fatigue crack growth evaluation.

The fatigue crack growth rate (da/dN) for the ferritic pressurizer material is a function of the range of applied stress intensity factor (ΔK_I) that can be expressed in the form of a Paris law as:

$$da/dN = C_o(\Delta K_I)^n$$

where:

a	=	flaw depth
N	=	number of stress cycles
C_o and n	=	experimentally determined parameters related to the material and operating environment
ΔK_I	=	stress intensity factor range (K_{max} - K_{min})

Since the postulated flaws are exposed to the internal pressurizer environment, the ASME Code fatigue crack growth curve for carbon and low alloy ferritic steels in water environments is used for the fatigue crack growth evaluation.

All the crack growth analyses are performed with the **pc-CRACK™ for Windows** fracture mechanics analysis program [22].

5.5 Results of Fatigue Crack Growth Analysis

The fatigue crack growth results are summarized in Tables 5-4 through 5-7 and illustrated in Figures 5-1 through 5-4 for the four small bore nozzles evaluated.

The postulated initial flaw in both of the bottom head nozzles grew beyond the modeled flaw analyzed in Section 3 after 45 years of fatigue crack growth. Thus, the resulting end-of-evaluation flaws have been evaluated by EPFM in Section 4. The postulated initial flaw in the side shell temperature and top head instrument nozzles grew by a very small amount after 45 years. Therefore, for each of the nozzles under consideration, the potential remnant crack is shown to grow by fatigue cycling during a period of 45 years of plant operation to a final end-of-evaluation period flaw size which has been shown to be acceptable in accordance with the flaw evaluation principles of ASME Section XI.

Table 5-1

Plant Design Transients for Pressurizer Bottom Head Nozzles

Transient ID	Description	# Cycles 40 years	# Cycles per year
HCHP_50 (Cooldown - Heatup)	High Pressure Insurge/Outsurge, ΔT = 50°F	290	8
HCHP_100 (Cooldown - Heatup)	High Pressure Insurge/Outsurge, ΔT = 100°F	120	3
HCHP_150 (Cooldown - Heatup)	High Pressure Insurge/Outsurge, ΔT = 150°F	500	13
HCLP_100 (Cooldown - Heatup)	Low Pressure Insurge/Outsurge, ΔT = 100°F	100	3
HCLP_150 (Cooldown - Heatup)	Low Pressure Insurge/Outsurge, ΔT = 150°F	75	2
HCLP_200 (Cooldown - Heatup)	Low Pressure Insurge/Outsurge, ΔT = 200°F	75	2
HCLP_250 (Cooldown - Heatup)	Low Pressure Insurge/Outsurge, ΔT = 250°F	290	8
HCLP_300 (Cooldown - Heatup)	Low Pressure Insurge/Outsurge, ΔT = 300°F	220	6
HCLP_350 (Cooldown - Heatup)	Low Pressure Insurge/Outsurge, ΔT = 350°F	120	3
TRIP (Trip – Steady State)	Reactor Trip at Max. Pressure (Case B)	480	12
TRIP (Trip – Steady State)	Max. Reactor Trip (Case A)	480	12

Table 5-2

Plant Design Transients for Pressurizer Side Shell Nozzles

Transient (Pressure)	Design Cycles for 40 Years	Average Cycles/Year	Cycles/Year used in pc-CRACK
Normal Heatup & Cooldown (2,250 psi)	500	12.5	13
Surge Heatup & Cooldown (401.6 psi)	100	2.5	3
Reactor Trip (1,800 psi)	480	12	12

Table 5-3

Plant Design Transients for Pressurizer Top Head Instrument Nozzle

Transient	Design Cycles for 40 Years	Cycles for 45 Years	Average Cycles/Year	Cycles/Year used in pc-CRACK
Heatup	500	562.5	12.5	13
Cooldown	500	562.5	12.5	13
Trip	480	540	12	12

Table 5-4

Fatigue Crack Growth Results – Bottom Head Heater Sleeve Nozzle

Location	Initial Crack Depth (in)	Final Crack Depth (in)	pc-CRACK Crack Growth (in)	Time (years)	End-of-Evaluation Period Stress Intensity Factor (ksi-in$^{1/2}$)									
					Trip - Steady	CD – HU, High Pressure (2,250 psi)			CD – HU, Low Pressure (401.6 psi)					
					NA	ΔT = 50°F	ΔT = 100°F	ΔT = 150°F	ΔT = 100°F	ΔT = 150°F	ΔT = 200°F	ΔT = 250°F	ΔT = 300°F	ΔT = 350°F
Downhill (Trip at Max. Press.) (Case B)	0.438	2.500	2.062	22	136.0	142.0	143.0	143.0	77.3	86.4	94.9	103.0	110.0	117.0
Uphill (Trip at Max. Press.) (Case B)	0.439	1.004	0.565	45	58.2	57.7	63.0	68.0	50.6	56.7	62.5	67.8	72.7	77.2
Downhill (Max. Trip) (Case A)	0.438	2.621	2.183	21	151.0	144.0	144.0	143.0	76.0	84.7	92.7	100.0	107.0	113.0
Uphill (Max. Trip) (Case A)	0.439	1.027	0.588	45	61.5	57.5	62.8	67.7	50.2	56.3	62.0	67.4	72.2	76.7

Table 5-5

Fatigue Crack Growth Results – Bottom Head Instrument Nozzle

Location	Initial Crack Depth (in)	pc-CRACK Final Crack Depth (in)	Crack Growth (in)	Time (years)	End-of-Evaluation Period Stress Intensity Factor (ksi-in$^{1/2}$)									
					Trip - Steady	CD – HU, High Pressure (2,250 psi)			CD – HU, Low Pressure (401.6 psi)					
					NA	ΔT = 50°F	ΔT = 100°F	ΔT = 150°F	ΔT = 100°F	ΔT = 150°F	ΔT = 200°F	ΔT = 250°F	ΔT = 300°F	ΔT = 350°F
Downhill (Trip at Max. Press.) (Case B)	0.442	1.472	1.030	45	57.8	48.4	60.1	70.8	16.8	24.1	30.8	36.9	42.4	47.6
Uphill (Trip at Max. Press.) (Case B)	0.438	1.387	0.949	45	106	98.1	107	116	76.7	82.6	88.0	93.0	97.6	102
Downhill (Max. Trip) (Case A)	0.442	1.394	0.952	45	49.5	52.9	64.8	75.7	22.7	30.2	37.0	43.3	48.8	54.1
Uphill (Max. Trip) (Case A)	0.438	1.327	0.889	45	96.9	98.7	108	117	77.9	84.0	89.6	94.8	99.5	104

Table 5-6

Fatigue Crack Growth Results – Side Shell Temperature Instrument Nozzle

Crack Tip Location	Initial Crack Depth (in)	Final Crack Depth (in)	Pc-CRACK Crack Growth (in)	Time (years)	End-of-Evaluation Period Stress Intensity Factor (ksi-in$^{1/2}$)		
					Normal Cooldown - Heatup	Surge Cooldown - Heatup	Trip
104	0.746	0.804	0.0580	45	26.3	49.9	35.9
133	0.7190	0.8172	0.0982	45	37.6	51.0	55.6

Table 5-7

Fatigue Crack Growth Results – Top Head Instrument Nozzle

Location	Initial Crack Depth (in)	pc-CRACK Final Crack Depth (in)	Crack Growth (in)	Time (years)	End-of-Evaluation Period Stress Intensity Factor (ksi-in$^{1/2}$)		
					Heatup	Cooldown	Trip
Uphill	0.844	0.872	0.028	45	36.1	27.7	50.8
Downhill	0.786	0.817	0.031	45	36.4	27.8	51.9

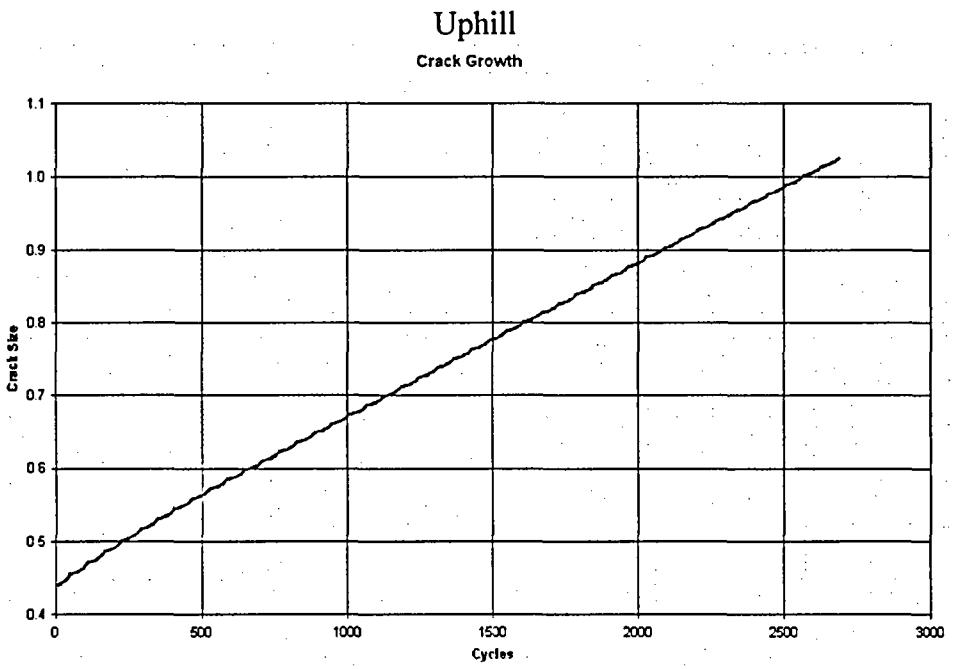

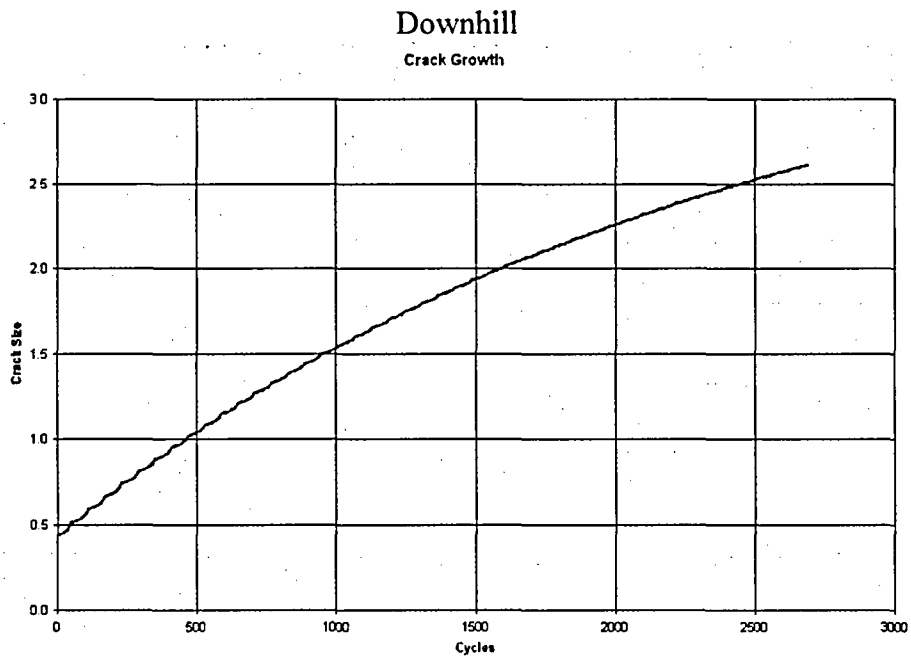

Figure 5-1. Fatigue Crack Growth Results, Bottom Head Heater Sleeve Nozzle Uphill and Downhill Locations

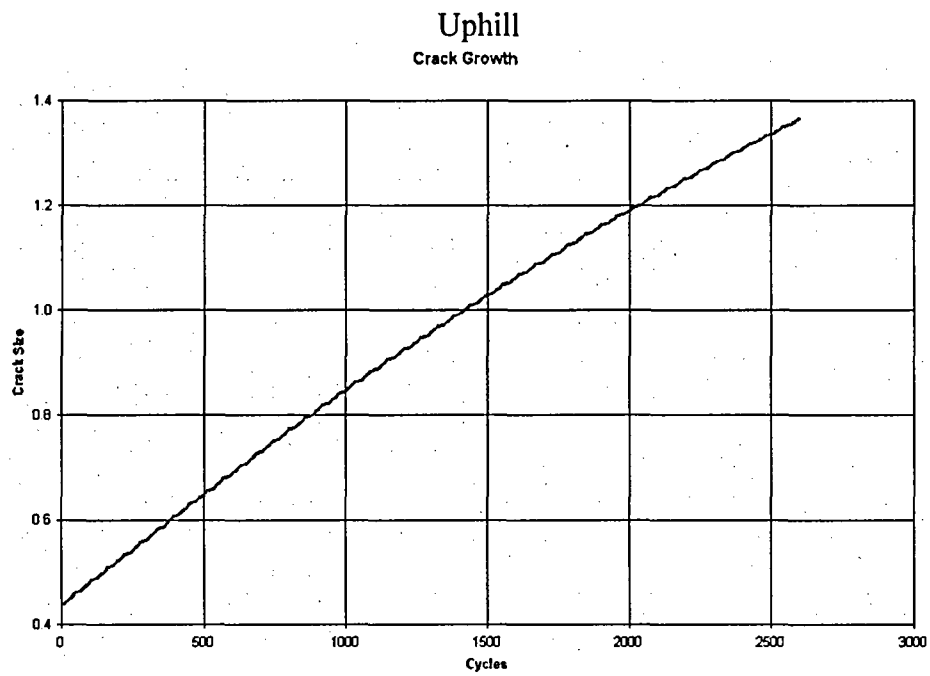

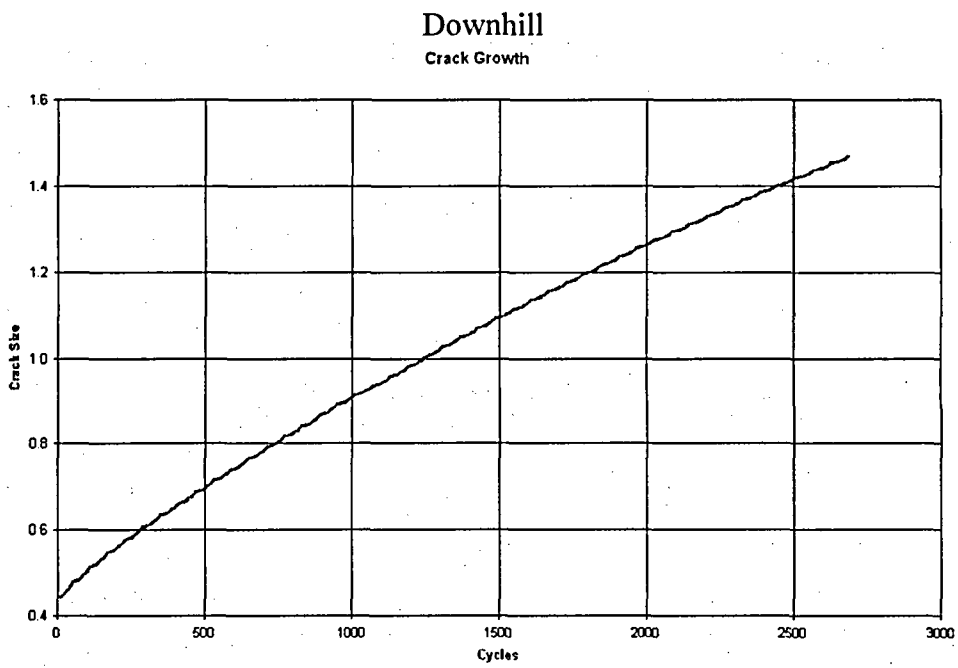

Figure 5-2. Fatigue Crack Growth Results, Bottom Head Instrument Nozzle Uphill and Downhill Locations

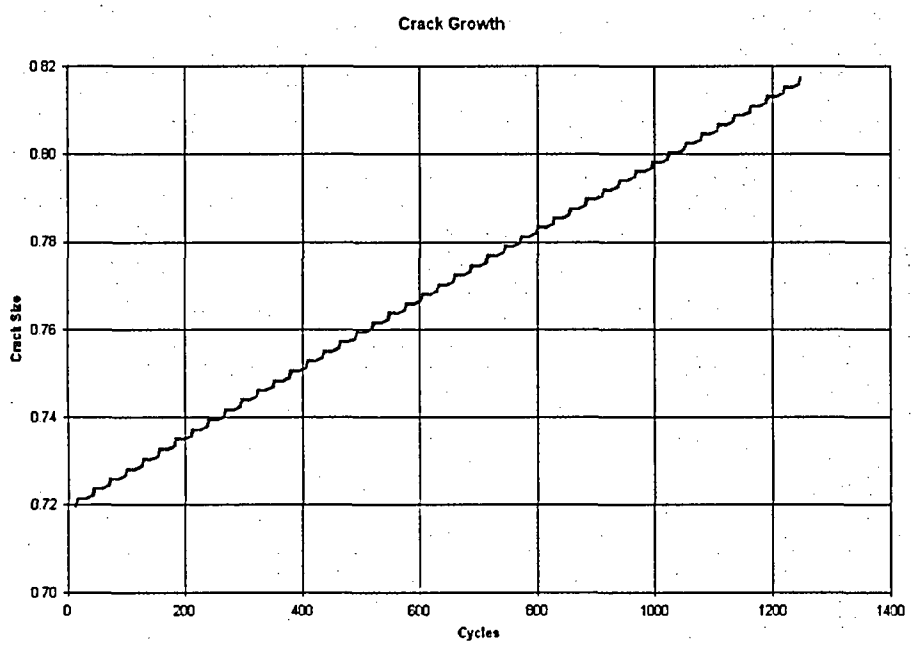

Figure 5-3. Fatigue Crack Growth Results, Side Shell Temperature Nozzle

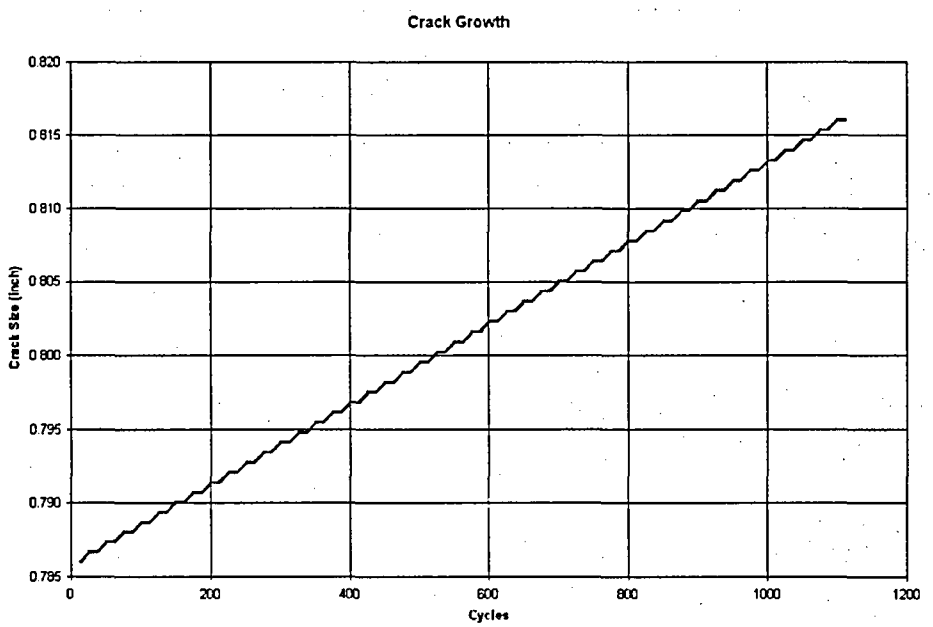

Figure 5-4. Fatigue Crack Growth Results, Top Head Instrument Nozzle

6.0 CONCLUSION

Fracture mechanics evaluations have been performed to qualify the repair designs for the Alloy 600 small bore nozzles in the Waterford-3 pressurizer. The evaluations showed that the potential remnant defect in the pressurizer bottom head heater sleeve, bottom head instrument, side shell temperature and top head instrument nozzle penetrations are acceptable based on either the LEFM or EPFM principles of Section XI of the ASME Code. Fatigue crack growth analyses were also performed and it was found that the postulated remnant flaws in the pressurizer small bore nozzle penetrations were acceptable for 45-year plant operating period.

7.0 REFERENCES

1. Structural Integrity Calculation WSES-10Q-301, Rev. 0, "Finite Element Model of Waterford-3 Pressurizer Bottom Head Small Bore Nozzle Repairs."
2. Structural Integrity Calculation WSES-10Q-304, Rev. 0, "Waterford-3 Pressurizer Small Bore Nozzle Repairs Thermal Stress Evaluations."
3. SI Calculation Package WSES-10Q-307, Rev. 0, "Finite Element Stress Analysis of the Waterford-3 Side Shell Temperature Nozzle Repair."
4. SI Calculation Package ENTP-13Q-327, Rev. 0, "Fracture Mechanics Evaluation of Waterford-3 Pressurizer Top Head Instrument Nozzle."
5. Westinghouse Calculation No. CN-OA-04-53, Rev. 0, "Evaluation of Insurges and Outsurges on the Pressurizer Lower Head During Plant Heatup and Cooldown Evolutions at Waterford-3," SI File No. WSES-10Q-220P.
6. SI Calculation Package, WSES-10Q-315, Rev. 0, "Fracture Mechanics Evaluation of Instrument Nozzle Penetration."
7. SI Calculation Package, WSES-10Q-316, Rev. 0, "Fracture Mechanics Evaluation of Outer-most Heater Sleeve Penetration with Entire Clad Cracked."
8. SI Calculation Package, WSES-10Q-317, Rev. 0, "LEFM Analysis of the Waterford-3 Side Shell Temperature Nozzle Repair."
9. ASME Boiler and Pressure Vessel Code, Section XI, 2001 Edition.
10. PVP2005-71718, Proceedings of PVP2005, 2005 ASME Pressure Vessels and Piping Division Conference, "Technical Basis for Revised Flaw Acceptance Criteria under IWB-3610 of ASME Section XI," July 17-21, 2005, Denver, Colorado USA.
11. Waterford FSAR, Unit 3, Table 5.2-8.
12. SI Calculation Package, WSES-16Q-303, Rev. 0, "EPFM Evaluation of Potential Remnant Crack in Waterford-3 Pressurizer Bottom Head Instrument Nozzle Repairs."
13. SI Calculation Package, WSES-16Q-304, Rev. 0, "EPFM Evaluation of Potential Remnant Crack in Waterford-3 Pressurizer Bottom Head Heater Sleeve Nozzle Repairs."
14. NUREG-0744, Vol. 2, Rev. 1, "Resolution of the Task A-11 Reactor Vessel Materials Toughness Safety Issue," Appendices C-K, Division of Safety Technology, Office of Nuclear Reactor Regulation, U.S. Nuclear Regulatory Commission, Washington, D.C. 20555, October 1982.
15. F. Loss, ed., "Structural Integrity of Water Reactor Pressure Boundary Components," USNRC Report NUREG/CR-1128, 1979.
16. Lowe, A. L., Napolitano, R. E., Spaar, D. M., and Stagg, W. R., "Analysis of Capsule W-97 Entergy Operations, Inc. Waterford Generating Station, Unit No. 3," B&W Nuclear Service Company, BAW-2177, November 1992.

17. SI Calculation Package, WSES-10Q-318, Rev. 0, "Fatigue Crack Growth Evaluation of Waterford-3 Pressurizer Instrument Nozzle Penetration—with 3 Flaw Configurations."

18. SI Calculation Package WSES-10Q-320, Rev. 0, "Fatigue Crack Growth Evaluation of Waterford-3 Pressurizer Heater Sleeve Nozzle Penetrations—with 4 Flaw Configurations."

19. SI Calculation Package WSES-10Q-321, Rev. 0, "Fatigue Crack Growth Evaluation of Waterford-3 Side Shell Temperature Nozzle."

20. SI Calculation Package WSES-16Q-305, Rev. 0, "Fatigue Crack Growth Evaluation of Waterford-3 Pressurizer Top Head Instrument Nozzle Penetration."

21. Combustion Engineering, "General Specification for a Pressurizer Assembly," Specification No. 00000-PE-130, Rev. 2, SI File No. ENTP-13Q-224P.

22. **pc-CRACK** for Windows, Version 3.1-98348, Structural Integrity Associates, 1998.

23. SI Calculation Package, WSES-10Q-309, Rev. 0, "Residual Stress Evaluation of the Pressurizer Sidewall Temperature Nozzle J-Groove Weld."

24. SI Calculation Package, WSES-10Q-311, Rev. 0, "Residual Stress Evaluation of the Pressurizer Bottom Head Instrument Nozzle J-Groove Weld."

25. SI Calculation Package, WSES-10Q-312, Rev. 0, "Residual Stress Evaluation of the Pressurizer Bottom Head Heater Sleeve J-Groove Weld."

26. Entergy Document No. CEXO-2003-00211, "Proposed Cooldown Curve Transients for ANO-2 and Waterford-3," Dated May 15, 2003, SI File No. W-ENTP-13Q-225.